A SARS-CoV-2 neutralizing antibody with exceptional spike binding coverage and optimized therapeutic potentials

Yu Guo (guoyu@nankai.edu.cn)
Nankai University https://orcid.org/0000-0002-8109-7515

Lisu Huang
Xinhua Hospital

Guangshun Zhang
Nankai University

Yanfeng Yao
Chinese Academy of Sciences

He Zhou
HiFibio(Hong Kong) Limited

Shu Shen
State Key Laboratory of Virology, Wuhan Institute of Virology, Chinese Academy of Sciences, Wuhan 430071 https://orcid.org/0000-0002-0013-5365

Bingqing Shen
HiFiBio(Hong Kong) Limited

Bo Li
Nankai University

Xin Li
Nankai University

Mingjie Chen
HiFiBio(Hong Kong) Limited

Da Chen
Nankai University

Jia Wu
HiFiBio(Hong Kong) Limited

Dan Fu
Nankai University

Xinxin Zeng
Xinhua Hospital

Mingfang Feng
HiFiBio(Hong Kong) Limited

Chunjiang Pi
HiFiBio(Hong Kong) Limited
Yuan Wang
Nankai University
Xingdong Zhou
Nankai University https://orcid.org/0000-0001-8648-8948
Minmin Lu
HiFiBio(Hong Kong) Limited
Yaohui Fang
Wuhan Institute of Virology
Yun-Yueh Lu
HiFiBio(Hong Kong) Limited
Xue Hu
Wuhan Institute of Virology, Center for Biosafety Mega-Science, Chinese Academy of Sciences
Shanshan Wang
HiFiBio(Hong Kong) Limited
Wanju Zhang
Shanghai Public Health Clinical Center, Fudan University
Qian Zhang
HiFiBio(Hong Kong) Limited
Ge Gao
Wuhan Institute of Virology, Center for Biosafety Mega-Science, Chinese Academy of Sciences
Francisco Adrian
HiFiBio(Hong Kong) Limited
Qisheng Wang
Shanghai Synchrotron Radiation Facility, Shanghai Advanced Research Institute, Chinese Academy of Sciences
Feng Yu
Shanghai Synchrotron Radiation Facility, Shanghai Advanced Research Institute, Chinese Academy of Sciences
Yun Peng
Wuhan Institute of Virology, Center for Biosafety Mega-Science, Chinese Academy of Sciences
Alexander Gabibov
Shemyakin-Ovchinnikov Institute of Bioorganic Chemistry
Juan Min
Wuhan Institute of Virology, Center for Biosafety Mega-Science, Chinese Academy of Sciences
Yuhui Wang
Nankai University
Heyu Huang

Xinhua Hospital
Alexey Stepanov
Shemyakin-Ovchinnikov Institute of Bioorganic Chemistry https://orcid.org/0000-0003-1616-4408
Wei Zhang
Nankai University https://orcid.org/0000-0001-8693-6747
Yan Cai
Tianjin International Joint Academy of Biotechnology & Medicine
Junwei Liu
Tianjin International Joint Academy of Biotechnology & Medicine
Zhi-Ming Yuan
Wuhan Institute of Virology https://orcid.org/0000-0002-3234-9616
Chen Zhang
Nankai University
Zhiyong Lou
Tsinghua University https://orcid.org/0000-0003-2728-881X
Fei Deng
State Key Laboratory of Virology, Wuhan Institute of Virology, Chinese Academy of Sciences, Wuhan 430071 https://orcid.org/0000-0002-5385-083X
Hongkai Zhang
Nankai University
Chao Shan
Chinese Academy of Sciences https://orcid.org/0000-0002-3953-3782
Liang Schweizer
HiFiBio(Hong Kong) Limited
Kun Sun
Xinhua Hospital
Zihe Rao
Tsinghua University https://orcid.org/0000-0001-9866-2384

Article

Keywords: SARS-CoV-2, spike glycoprotein, neutralizing antibody, antibody engineering, structure analysis, in vivo efficacy

Posted Date: November 14th, 2020

DOI: https://doi.org/10.21203/rs.3.rs-78945/v1

Version of Record: A version of this preprint was published at Nature Communications on May 11th, 2021. See the published version at https://doi.org/10.1038/s41467-021-22926-2.

A SARS-CoV-2 neutralizing antibody with exceptional spike binding coverage and optimized therapeutic potentials

Yu Guo[1,7,12,*,$], Lisu Huang[2,$], Guangshun Zhang[1,4,$], Yanfeng Yao[5,$], He Zhou[3,$], Shu Shen[7,$], Bingqing Shen[3], Bo Li[1,4], Xin Li[1,4], Mingjie Chen[3], Da Chen[1,4], Jia Wu[3], Dan Fu[1], Xinxin Zeng[2], Mingfang Feng[3], Chunjiang Pi[3], Yuan Wang[1,4], Xingdong Zhou[1,4], Minmin Lu[3], Yaohui Fang[7], Yun-Yueh Lu[3], Xue Hu[7], Shanshan Wang[3], Wanju Zhang[2], Qian Zhang[3], Ge Gao[5], Francisco Adrian[3], Qisheng Wang[10], Feng Yu[10], Yun Peng[5], Alexander G. Gabibov[11], Juan Min[5], Yuhui Wang[1,4], Heyu Huang[2], Alexey Stepanov[11], Wei Zhang[1,4], Yan Cai[6], Junwei Liu[6], Zhiming Yuan[5], Chen Zhang[1], Zhiyong Lou[8,*], Fei Deng[7,*], Hongkai Zhang[1,4,9,12*], Chao Shan[7,*], Liang Schweizer[3,*], Kun Sun[2,*], Zihe Rao[1,4,*]

[1] State Key Laboratory of Medicinal Chemical Biology and College of Pharmacy, Nankai University, 38 Tongyan Road, Tianjin, 300071, China

[2] Xinhua Hospital, Shanghai Jiao Tong University School of Medicine, Shanghai, China.

[3] HiFiBio (Hong Kong) Limited, 2 Ice House Street, Central, Hong Kong

[4] College of Life Science, Nankai University, 94 Weijin Road, Tianjin, 300071, China

[5] Center for Biosafety Mega-Science, Wuhan Institute of Virology, Chinese Academy of Sciences, Wuhan, Hubei 430071, China.

[6] Tianjin International Joint Academy of Biotechnology & Medicine, Tianjin 300457, People's Republic of China

[7] State Key Laboratory of Virology and National Virus Resource Center, Wuhan Institute of Virology, Chinese Academy of Sciences, Wuhan, Hubei 430071, China

[8] MOE Key Laboratory of Protein Science & Collaborative Innovation Center of Biotherapy, School of Medicine, Tsinghua University, Beijing, China

[9] Shanghai Institute for Advanced Immunochemical Studies, ShanghaiTech University, Shanghai, 201210, P.R. China

[10] Shanghai Synchrotron Radiation Facility, Shanghai Advanced Research Institute, Chinese Academy of Sciences, Shanghai 201204, China

[11] Shemyakin-Ovchinnikov Institute of Bioorganic Chemistry, Russian Academy of Sciences, 117997 Moscow, Russia

[12] Frontiers Science Center for Cell Responses, Nankai University, 94 Weijin Road, Tianjin, 300071, China

[$] These authors contribute equally to this work

* Correspondence should be sent to: Z.R (raozh@mail.tsinghua.edu.cn),

K.S(sunkun@xinhuamed.com.cn), L.S (l.schweizer@hifibio.com);

C.S(shanchao@wh.iov.cn), H.Z(hongkai@nankai.edu.cn), , F.D(df@wh.iov.cn),

Z.L(louzy@mail.tsinghua.edu.cn) and Y.G(guoyu@nankai.edu.cn)

Abstract

The Coronavirus Disease of 2019 (COVID-19) pandemic caused by severe acute respiratory syndrome coronavirus 2 (SARS-CoV-2) threatens global public health and economy. Therapeutic options such as monoclonal antibodies (mAbs) against SARS-CoV-2 are in urgent need. We have identified potent monoclonal antibodies binding to SARS-CoV-2 Spike protein from COVID-19 convalescent patients and one of these antibodies, P4A1, interacts directly and covers the majority of the Receptor Binding Motif (RBM) of Spike receptor-binding domain (RBD), shown by high-resolution complex structure analysis. We further demonstrated P4A1 binding and neutralizing activities against wild type and mutant spike proteins. P4A1 was subsequently engineered to reduce the potential risk for antibody-dependent enhancement (ADE) of infection and to extend its half-life. The engineered mAb exhibits optimized pharmacokinetic and safety profile, and results in complete viral clearance in a rhesus monkey model of COVID-19 following a single injection.

Keywords:

SARS-CoV-2, spike glycoprotein, neutralizing antibody, antibody engineering, structure analysis, in vivo efficacy

Introduction

COVID-19 has recently emerged throughout the world as the largest pandemic of the 21st century, with over 35 million confirmed cases and over 1 million deaths worldwide as of Oct. 7th, 2020, which requires urgent prophylactic and treatment options. Like other Class I fusion proteins, the spike (S) glycoprotein forms homotrimers on the surface of SARS-CoV-2 virus particle, mediates the recognition and binding to the human receptor, angiotensin-converting enzyme 2 (hACE2), through its receptor-binding domain (RBD), and induces the virus-host cell membrane fusion, and serves as the primary target for interfering the virus entry process(*1*). A number of SARS-CoV-2 vaccines currently under development have shown successful induction of anti-viral antibodies in clinical trials (*2-4*). The final success of anti-SARS-CoV-2 vaccines may be depending on the quality of immune responses induced, particularly in elderly or individuals with pre-existing conditions, or the willingness to accept vaccination. Recent reports of SARS-CoV-2 reinfection in patients brought new challenges to the vaccine approaches.

To date, many efforts have been devoted to the discovery and development of SARS-CoV-2 neutralizing antibodies using various platforms, including antibody isolation and screening from SARS-CoV(*5, 6*) or SARS-CoV-2 convalescent patients(*7-16*), humanized mice(*17, 18*), and phage libraries(*19, 20*). Among them, several leading antibodies have entered the clinical trial stage. Of note, a major

concern for the development of vaccine or neutralizing antibody therapies is the potential risk of antibody-dependent enhancement (ADE) of infection (*21, 22*), which also previously reported in infections of viruses such as dengue(*23*) and SARS-CoV(*24*), and raised as a concern for SARS-CoV-2 countermeasures (*15, 25*). Another aspect to consider is the ability of the evolving virus to mutate and escape from treatments. To date, about 19 mutation sites in the Spike protein have been described from an online database tracing ~65k documented sequences (https://cov.lanl.gov/content/index), of which D614G has become the most prevalent form in the global pandemic(*26*), the development of potent treatments effective to different SARS-CoV-2 mutants is urgently needed.

Results

To identify SARS-CoV-2 neutralizing antibodies from convalescent patients, we utilized a high-throughput single-cell B-cell receptor sequencing approach. SARS-CoV-2 neutralizing antibodies were isolated from the two convalescent patients with the highest titer against S protein (patient #4 and patient # 20) among 23 patients studied (Fig. S1A). SARS-CoV-2 S protein binding B cells from PBMCs were enriched with biotinylated S protein conjugated magnetic beads as probes as described (Fig. S1C and S1D). Among the sequenced antibodies, P4A1, P20A2 and P20A3 were shown to bind to the S1 subunit with sub-to-nM EC_{50}s, but not to the S2 subunit, and blocked the binding of the S1 subunit to hACE2 with IC_{50} values in the sub-to-nM range

(Fig.1A). P4A1, P20A2, P20A3 neutralized the live SARS-CoV-2 infection of Vero-E6 cells with ND_{50} values of 5.212, 43.79, and 29.03 nM, respectively (Fig. 1B). According to the ImmunoGenetics (IMGT) database-based analysis, IGHV3-53 was assigned as the antibody P4A1's IGHV germline origin, which has been proved to be one of the most frequent used germlines after SARS-CoV-2 infection in patients(*16*) (Fig. S3 and S4A).

To gain further insight into the structural basis for the blocking and neutralizing mechanism of P4A1, the structure of the antibody Fab/Spike-RBD complex was resolved by X-ray crystallography at the resolution of 2.1 Å (Fig.2A, Table.S1). Three heavy chain complementarity-determining regions (HCDRs), two light chain complementarity-determining regions (LCDRs), together with weak interaction from the light chain framework region 3 (LFR3) constitute the interaction network with SARS-CoV-2 RBD (Fig.2B). The buried surface area (BSA) from the heavy-chain interaction in P4A1 (781 $Å^2$) is relatively larger compared to reported neutralizing antibodies including CC12.1 (723 $Å^2$), CC12.3 (698 $Å^2$)(*16*), CB6(734 $Å^2$)(*14*) and B38 (713 $Å^2$)(*14*) (Fig.S3); However, the BSA from the light chain varies significantly, with P4A1 (577 $Å^2$) being the largest compared to CC12.1 (566 $Å^2$), CC12.3 (176 $Å^2$)(*16*), CB6 (334 $Å^2$)(*15*) and B38 (495 $Å^2$)(*14*). Specifically, the interaction network is mainly contributed by hydrogen bond and hydrophobic interaction. For the heavy chain, P4A1 HCDR1 and HCDR2 shares similar interaction pattern with SARS-CoV-2 Spike RBD as CC12.1 and CC12.3, while these antibodies differ in their HCDR3 sequence, with

Q100, E101 forming hydrogen bond with K417 and Y453, and the side chain of L102 inserts into the hydrophobic cavity formed by L485, F456 and Y489 (Fig. 2C, upper panel); For the light chain, the hydrogen bond network is mediated by G28, S30, S31 W32 in LCDR1 with T500, N501, G502, Q498, Y449, and G496; and E90, N92, S93 in LCDR3 with Y505, and R403(Fig. 2C, lower panel). It is worth noting that the water molecule plays more important role for light chain than it does for the heavy chain.

P4A1 Fab locates directly at the Receptor Binding Motif (RBM) region of SARS-CoV-2 Spike RBD, hence inducing steric hindrance to the binding of receptor hACE2 (Fig. 2A). Except for residues G446 and Y449, 15 of the 17 residues identified as SARS-CoV-2 Spike RBD-hACE2 binding sites(*1*) are within P4A1 epitope using the distance of <4 Å as the cutoff, while Y449 is exactly 4 Å from P4A1 (Fig. 2B, Table S2). This represents one of the most extensive coverages of residues involved in the Spike-hACE2 interaction to date and may explain potent neutralization activity for P4A1. This broad coverage may suggest effectiveness against viral mutants as mutations to hACE2 epitopes on Spike protein are rare in clinical isolates because of their importance in viral infectivity. Structure analysis showed that all 8 residues with reported mutations in the Spike RBD of clinical isolates (*27*), are mostly located far away from P4A1 epitope (Fig. S4B), are expected to have no or minimal effects on the binding and neutralization activity of P4A1. This was supported by the test of P4A1 binding ability to wild type, different RBD mutants and D614G variants of S1 protein by SPR (Fig. 3A) or ELISA (Fig. S5), as well as neutralization of pseudoviruses

143 expressing wildtype or D614G, V367F, D264Y or W436R variants of Spike protein with
144 similar IC_{50}s (Fig. 3B).

145 To facilitate its clinical applications, P4A1 was further engineered as an IgG4
146 antibody (named as P4A1-2A) to reduce the risks of Fcγ- or complement-receptor-
147 mediated ADE with modifications to reduce Fab-arm exchange(*28*), and to increase
148 antibody blood half-life in primates. Consistent with its isotype and Fc engineering,
149 P4A1-2A displayed 4-81 fold decrease in binding affinity to different FcγRs, no binding
150 to complement C1q, and enhanced affinity for FcRn when compared to its IgG1 form
151 P4A1 (Fig. 3C and S6). The effect of enhanced FcRn binding is further validated by
152 the longer serum half-life in cynomolgus monkey (Fig. S6). The prolonged half-life is
153 highly desired as it will be beneficial for long-term protection in individuals at high risk
154 of contracting SARS-CoV-2 infection during the pandemic. Furthermore, the safety of
155 P4A1-2A was demonstrated in a GLP Toxicity study where cynomolgus monkeys were
156 treated with 2 weekly i.v infusions of up to 300 mg/kg/dose and no treatment-related
157 findings were observed in any of the tests performed, including cytokine levels, such
158 as IL-2, IL-6, IL-10, TNF-α and IFN-γ at different timepoints. Besides, no tissue cross-
159 reactivity was observed for 37 different normal human tissues.

160 The effectiveness of the engineered antibody was examined in a SARS-CoV-2
161 infection model in rhesus macaques (Figure 4A). Isotype control or P4A1-2A were
162 administered in a single intravenous (i.v.) infusion 1 day after intra-tracheal virus
163 inoculation at 1×10^5 $TCID_{50}$. Consistent with the previous report(*29*), in the isotype

control (50 mg/kg) group, viral load using oropharyngeal swabs was at high level 1 day post-infection (d.p.i.), showing the colonization of virus, decreased 2 d.p.i., suggesting viral distribution, increased 3-4 d.p.i. and maintained at high level through 7 d.p.i indicating viral replication. Importantly, in 3 out of 3 (50 mg/kg) and 2 out the 3 (10mg/kg) P4A1-2A-treated animals, the viral load dropped continuously to a level near or below the detection limit, and viral elimination occurred on 3-4 d.p.i., indicating effective blocking of viral propagation by P4A1-2A (Fig. 4B).

At necropsy, trachea, left and right bronchus and different lung lobes were isolated, homogenized and tested for viral load. Substantial viral load was detected in 5 or 6 out of the 9 tissues examined (including consistent viral presence in trachea, left and right bronchus) with moderate to severe lung lesions similar to previous report (*29*) in animals in the isotype control treatment group. In contrast, no viral load was detected 6 or 7 d.p.i in any of these tissues examined and with to mild-moderate lung lesions in the 50 mg/kg P4A1-2A-treated animals. In the 10 mg/kg P4A1-2A-treated animals, virus was detected in only 1 of the 9 tissues examined 7 d.p.i and no viral RNA detected in any of the lung tissues in all 3 animals (Fig. 4C, 4D and Fig S8).

These results represent similar or better anti-viral efficacy in the respiratory system than the currently reported antibodies(*15*) with lower i.v. dose of neutralizing antibody used in similar NHP SARS-CoV-2 infection models. In addition to the potency of P4A1-2A, a potentially better distribution to the respiratory tract associated with the engineered IgG4 antibodies by previous work(*30*) may contribute to the total viral

clearance in some of the animals. These data demonstrated that P4A1-2A was effective despite reduced FcγR effector functions.

Discussion

High affinity neutralizing antibodies from convalescent patients may represent some of the most efficient anti-viral weapons contributing to a patient recovery from viral infection. Given that not every COVID-19 patient is able to produce high quality antibodies such as P4A1, this antibody along with antibody engineering to reduce potential safety concerns and to prolong the serum half-life, may provide durable protection to every patient and, especially, to individuals at high risk of viral infection. The structural analysis demonstrates the molecular basis for neutralizing mechanism of P4A1, whose epitope include most of the binding residues of hACE2 and exhibited potent antiviral activities *in vitro* and *in vivo*. The broad coverage of hACE2 epitopes may contribute to effectiveness to viral mutants, supported by activities against all spike protein mutants tested, including the most prevalent variant D614G, with similar EC_{50}/IC_{50}s compared to wild type protein.

With prolonged half-life, potential for a broad spectrum of viral neutralization, P4A1-2A represents not only optimized therapeutic potency, but also an important prophylactic option to safeguard the vulnerable or aged populations, complementary to vaccine approaches. The comprehensive characterization of this antibody provides

strong evidence for its promising potential to effectively treat and prevent COVID-19 in humans.

References

1. J. Shang *et al.*, Structural basis of receptor recognition by SARS-CoV-2. *Nature* **581**, 221-224 (2020).
2. H. Wang *et al.*, Development of an Inactivated Vaccine Candidate, BBIBP-CorV, with Potent Protection against SARS-CoV-2. *Cell* **182**, 713-721 e719 (2020).
3. F. C. Zhu *et al.*, Immunogenicity and safety of a recombinant adenovirus type-5-vectored COVID-19 vaccine in healthy adults aged 18 years or older: a randomised, double-blind, placebo-controlled, phase 2 trial. *Lancet* **396**, 479-488 (2020).
4. P. M. Folegatti *et al.*, Safety and immunogenicity of the ChAdOx1 nCoV-19 vaccine against SARS-CoV-2: a preliminary report of a phase 1/2, single-blind, randomised controlled trial. *Lancet* **396**, 467-478 (2020).
5. D. Pinto *et al.*, Cross-neutralization of SARS-CoV-2 by a human monoclonal SARS-CoV antibody. *Nature* **583**, 290-295 (2020).
6. A. Z. Wec *et al.*, Broad neutralization of SARS-related viruses by human monoclonal antibodies. *Science* **369**, 731-736 (2020).
7. D. Zhou *et al.*, Structural basis for the neutralization of SARS-CoV-2 by an antibody from a convalescent patient. *Nat Struct Mol Biol*, (2020).
8. P. J. M. Brouwer *et al.*, Potent neutralizing antibodies from COVID-19 patients define multiple targets of vulnerability. *Science* **369**, 643-650 (2020).
9. Y. Cao *et al.*, Potent Neutralizing Antibodies against SARS-CoV-2 Identified by High-Throughput Single-Cell Sequencing of Convalescent Patients' B Cells. *Cell* **182**, 73-84 e16 (2020).
10. X. Chi *et al.*, A neutralizing human antibody binds to the N-terminal domain of the Spike protein of SARS-CoV-2. *Science* **369**, 650-655 (2020).
11. C. Kreer *et al.*, Longitudinal Isolation of Potent Near-Germline SARS-CoV-2-Neutralizing Antibodies from COVID-19 Patients. *Cell* **182**, 843-854 e812 (2020).
12. D. F. Robbiani *et al.*, Convergent antibody responses to SARS-CoV-2 in convalescent individuals. *Nature* **584**, 437-442 (2020).
13. T. F. Rogers *et al.*, Isolation of potent SARS-CoV-2 neutralizing antibodies and protection from disease in a small animal model. *Science* **369**, 956-963 (2020).
14. Y. Wu *et al.*, A noncompeting pair of human neutralizing antibodies block COVID-19 virus binding to its receptor ACE2. *Science* **368**, 1274-1278 (2020).
15. R. Shi *et al.*, A human neutralizing antibody targets the receptor-binding site of SARS-CoV-2. *Nature* **584**, 120-124 (2020).
16. M. Yuan *et al.*, Structural basis of a shared antibody response to SARS-CoV-2. *Science* **369**, 1119-1123 (2020).
17. J. Hansen *et al.*, Studies in humanized mice and convalescent humans yield a SARS-CoV-2 antibody cocktail. *Science* **369**, 1010-1014 (2020).

18. Z. Lv *et al.*, Structural basis for neutralization of SARS-CoV-2 and SARS-CoV by a potent therapeutic antibody. *Science*, (2020).
19. H. A. Parray *et al.*, Identification of an anti-SARS-CoV-2 receptor binding domain directed human monoclonal antibody from a naive semi-synthetic library. *J Biol Chem*, (2020).
20. Y. Wu *et al.*, Identification of Human Single-Domain Antibodies against SARS-CoV-2. *Cell Host Microbe* **27**, 891-898 e895 (2020).
21. A. M. Arvin *et al.*, A perspective on potential antibody-dependent enhancement of SARS-CoV-2. *Nature* **584**, 353-363 (2020).
22. W. Hoepel *et al.*, Anti-SARS-CoV-2 IgG from severely ill COVID-19 patients promotes macrophage hyper-inflammatory responses. *bioRxiv*, (2020).
23. L. C. Katzelnick *et al.*, Antibody-dependent enhancement of severe dengue disease in humans. *Science* **358**, 929-932 (2017).
24. M. S. Yip *et al.*, Antibody-dependent infection of human macrophages by severe acute respiratory syndrome coronavirus. *Virol J* **11**, 82 (2014).
25. L. M. Walker, D. R. Burton, Passive immunotherapy of viral infections: 'super-antibodies' enter the fray. *Nat Rev Immunol* **18**, 297-308 (2018).
26. B. Korber *et al.*, Tracking Changes in SARS-CoV-2 Spike: Evidence that D614G Increases Infectivity of the COVID-19 Virus. *Cell* **182**, 812-827 e819 (2020).
27. J. Ou *et al.*, Emergence of RBD mutations in circulating SARS-CoV-2 strains enhancing the structural stability and human ACE2 receptor affinity of the spike protein. 2020.2003.2015.991844 (2020).
28. A. F. Labrijn *et al.*, Therapeutic IgG4 antibodies engage in Fab-arm exchange with endogenous human IgG4 in vivo. *Nat Biotechnol* **27**, 767-771 (2009).
29. C. Shan *et al.*, Infection with novel coronavirus (SARS-CoV-2) causes pneumonia in Rhesus macaques. *Cell Res* **30**, 670-677 (2020).
30. W. F. Dall'Acqua, P. A. Kiener, H. Wu, Properties of human IgG1s engineered for enhanced binding to the neonatal Fc receptor (FcRn). *J Biol Chem* **281**, 23514-23524 (2006).

Correspondence

Z.R (raozh@mail.tsinghua.edu.cn), K.S(sunkun@xinhuamed.com.cn), L.S (l.schweizer@hifibio.com); C.S(shanchao@wh.iov.cn), H.Z(hongkai@nankai.edu.cn), F.D(df@wh.iov.cn), Z.L(louzy@mail.tsinghua.edu.cn) and Y.G(guoyu@nankai.edu.cn)

Acknowledgments

We thank the running team of National Biosafety Laboratory, staffs from Center for Instrumental Analysis and Metrology, Wuhan, Chinese Academy of Sciences, and staffs from BL-17U1, Shanghai Synchrotron Radiation Facility. We thank Cheryl Cui and Jeff He for their critical role in setting up collaboration among different institutions, Ning Zhang from Red Avenue Foundation for her support.

This work was supported by the National Program on Key Research Project of China (2018YFE0200400, 2018YFA0507203, 2017YFC840300, 2017YFA0504801 and 2020YFC0845801), the National Natural Science Foundation of China (NSFC) (31670731, 31870733), Projects of International Cooperation and Exchanges NSFC (grant no.81520108019), Medical and Industrial Cross Research Foundation of Shanghai Jiao Tong University (YG2020YQ27), and Science and Technology Innovation Achievements and Team Building Foundation of Nankai University (grant no. ZB19500403, ZB19100123 and 63201101).

Author contributions

Z. R., K.S., L.S., H.-K.Z., Z.-Y. L., and Y.G. conceived the project. L.-S.H. X.-X.Z., W.-J.Z., H.-Y.H. and K.S. collected the convalescent PBMC and serum and take responsibility for the human ethic issue. Y.G., L.-S.H., G.-S.Z., B.-Q.S., M.-J.C., J.W., M.-F.F., B.L., D.F., W.Z., Y.-H.W., Y.C., J.-W.L. and C.Z. performed gene construction, protein expression and purification, and crystal screening and optimization. Y.G., X.L., Q.-S.W., Q.Z., F.Y., A.S., and A.G.G. performed the collection of X-ray diffraction data and structure determination. L.-S.H., G.-S.Z., B.-Q.S., S.-S.W., Y.-Y.L., M.-M.L., C.-J.P., D.C., Y.W., and X.-D.Z. performed the in vitro binding assays and analysis data. S.S., Y.-H.F., and F.D. performed live virus neutralization assays. C.S., Y.F.Y., X.H., G.G., Y.P., J.M., and Z.-M.Y. performed animal assays. Y.G., H.-K.Z., L.S., H.Z., Z. R., K.S., and F.A. designed the experiments and wrote the manuscript. All authors read and approved the contents of the manuscript.

Competing interests

L.S., B.-Q.S., H.Z., M.-J.C., Y.-Y.L.; L.S.H.; K.S. are the inventors of the pending patent application filed on the reported antibodies. L.S., B.-Q.S., H.Z., M.-J.C., J.W., M.-F.F., C.-J.P., M.-M.L., Y.-Y.L.; S.-S.W., Q.Z., F.A. employees of HiFiBio (Hong Kong) Ltd. Other authors declare no competing interests. All reagents and information presented in this study are available from corresponding authors upon reasonable request.

Figures and Figure Legends

Figure 1

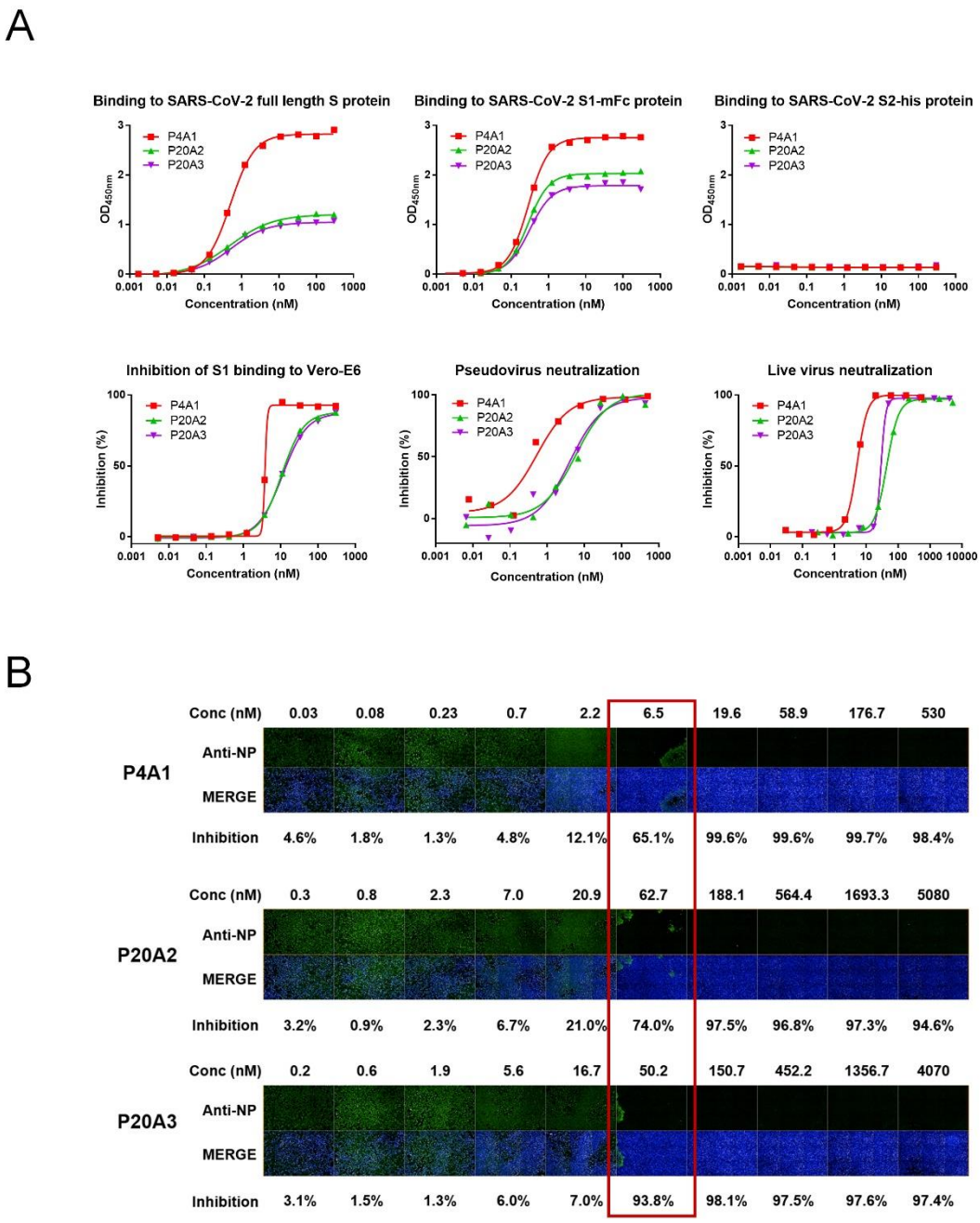

Figure 1. Characterization of neutralizing antibodies from convalescent patients. (A) Characterization of SARS-CoV-2 S protein specific antibodies. (upper panels) Binding of antibodies to the full-length S protein, S1 protein and S2 protein were evaluated by ELISA. (lower left panel) Blockage of the binding of SARS-CoV-2 spike S1 protein to Vero E6 cell

line by antibodies evaluated by flow cytometry. (Lower middle panel) Pseudovirus neutralization assay in Huh-7 cell line. (lower right panel and B) SARS-CoV-2 live virus neutralization assay. (B) Images of Vero E6 cells infected SARS-CoV-2 treated with antibodies of different concentrations.

Figure 2

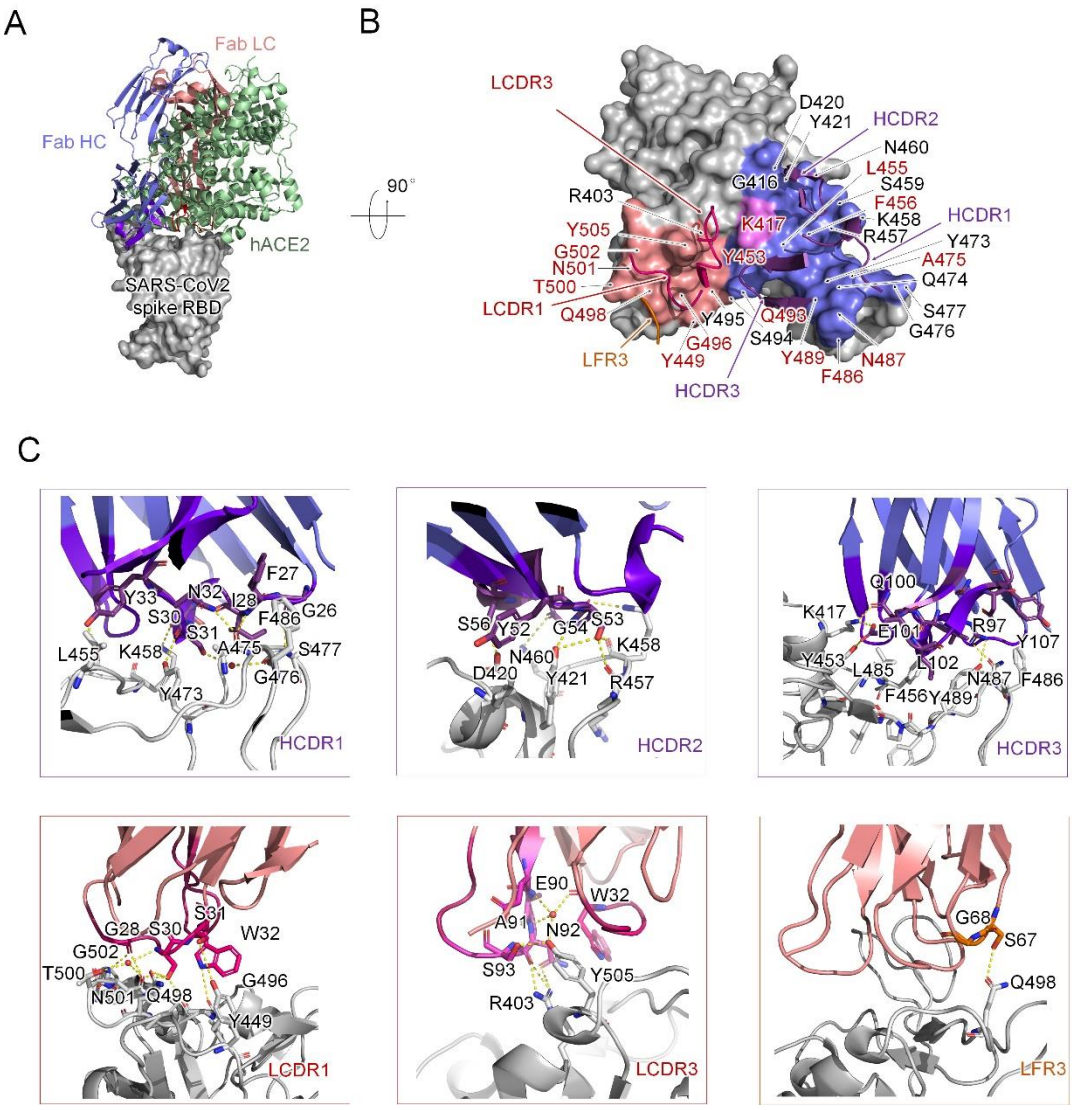

Figure 2. Structural analysis of P4A1 Fab and SARS-CoV-2 RBD complex. (A) The overall P4A1-Fab-RBD complex structure superimposed with the hACE2-RBD complex. The P4A1 heavy chain (colored slate blue), light chain (colored salmon red) and hACE (colored pale green) are displayed in cartoon representation. The SARS-CoV-2 RBD is colored in gray and displayed in surface representation. (B) The epitope of P4A1 shown in surface representation. The CDR loops of heavy chain (HCDR) and light chain (LCDR) are colored in purple and magenta, respectively. The epitopes from the heavy chain and light chain are colored in slate blue and salmon red, respectively. The only residue K417, which contacts with both heavy chain and light chain is colored in pink. The light chain frame region 3 (LFR3) is colored in orange. The identical residues on RBD shared in P4A1 and hACE2 binding are

338 labelled in red. The residues are numbered according to SARS-CoV-2 RBD. (C) The detailed
339 interactions between SARS-CoV-2 RBD with HCDR, LCDR and LFR3. The residues are
340 shown in sticks with identical colors to (B).
341

Figure 3

A

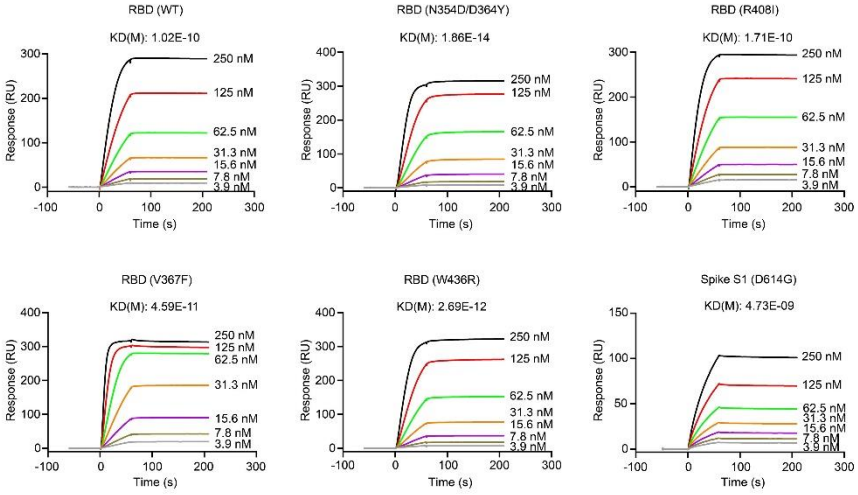

B

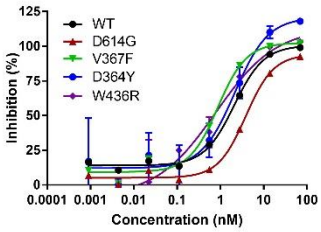

	WT	D614G	V367F	D364Y	W436R
IC_{50}(nM)	2.077	3.869	0.871	2.147	0.787

C

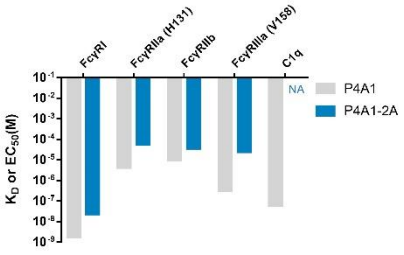

Figure 3. The activities of IgG4 antibody P4A1-2A to different SARS-CoV-2 S protein mutants, FcγRs and C1q. (A) Binding of antibody P4A1 to SARS-CoV-2 S protein N354D/D364Y, R408I, W436R, V367F or D614G mutants determined by SPR. (B) Pseudo virus neutralization assay in hACE2 overexpressing HEK293 cells. (C) The binding affinity of P4A1 and P4A1-2A for different human FcγRs and complement C1q.

353 **Figure 4**

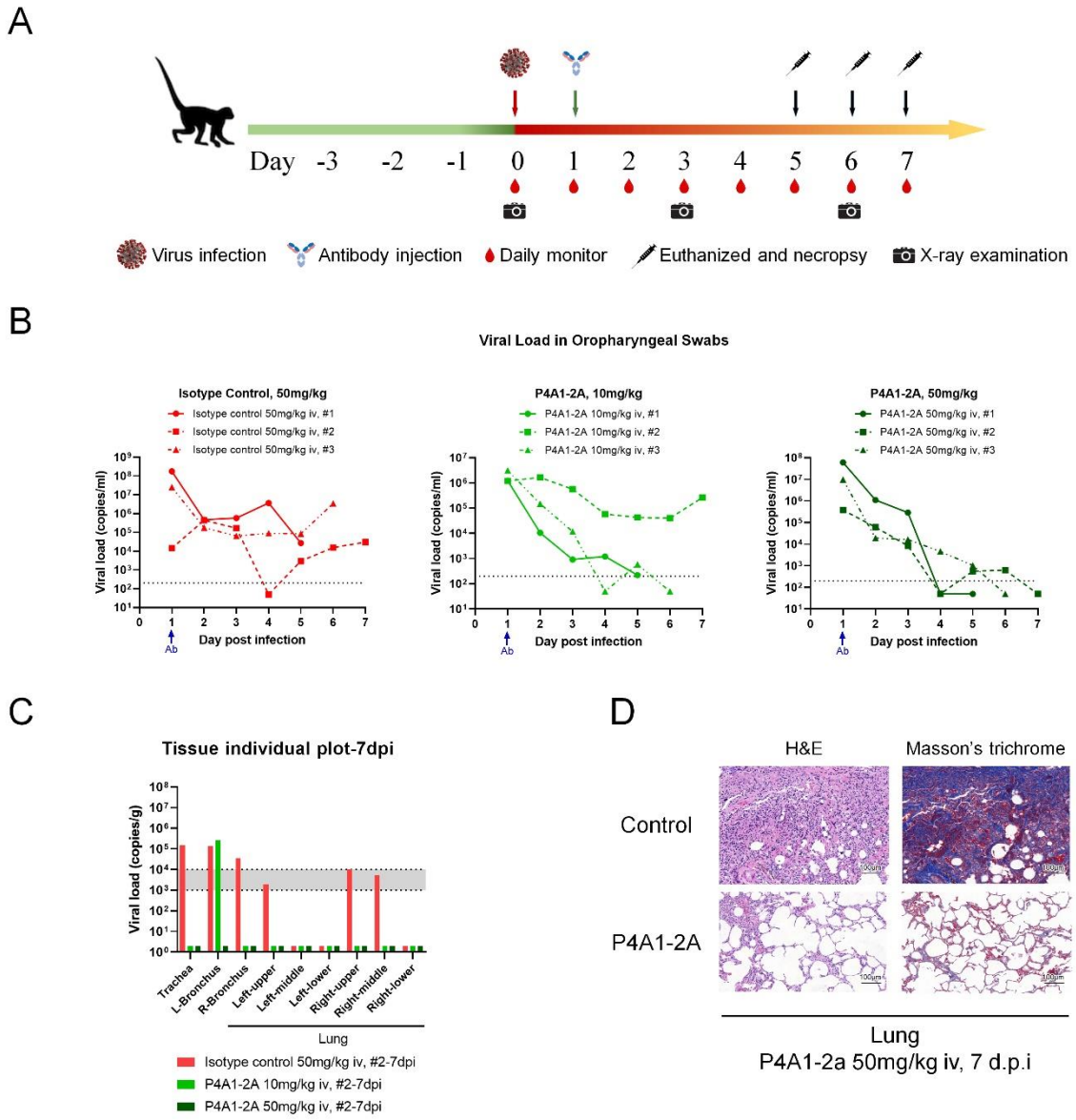

354

355 **Figure 4. Therapeutic efficacy of in the rhesus macaque model of SARS-CoV-2**
356 **infection.** (A) Experimental design for therapeutic testing of P4A1-2A in the rhesus
357 macaque. (B) Viral load in oropharyngeal swabs tested by RT-qPCR were monitored for 7
358 days. (C) Viral load in the respiratory tissues (including trachea, left and right bronchus, and
359 all six lung lobes) collected at necropsy on 7 days post-infection (d.p.i) were tested by RT-
360 qPCR. (D) Representative images of histopathology in lung tissue from isotype control or

P4A1-2A 50 mg/kg treated animals (collected at 7 d.p.i).

Methods

Ethics statements

The study was approved by the Ethics Committee of Xinhua Hospital affiliated to Shanghai Jiao Tong University (approval #XHEC-C-2020-006-2), Yongjia People's Hospital and Yongjia Center for Disease Control and Prevention in Zhejiang Province. Blood samples were collected from convalescent COVID-19 patients and healthy volunteers with signed informed consent forms according to study protocol approved by IRBs

All animal experiments were approved by the Institutional Animal Care and Use Committee (IACUC) of Wuhan Institute of Virology, Chinese Academy of Sciences (Ethics number: WIVA42202001) or Wuxi AppTec (Number: SZ20200529-Monkeys for PK study and SZ20200608-Monkeys for GLP Toxicology study). Rhesus macaque studies were conducted within the animal biosafety level 4 (ABSL- 4) facility in the National Biosafety Laboratory (Wuhan), Chinese Academy of Sciences.

Study design and participants

Convalescent COVID-19 patients were recruited between February 11th, 2020 and March 1st, 2020 at Yongjia People's Hospital and Yongjia Center for Disease Control and Prevention in Zhejiang Province, China. All the patients with COVID-19 were clinically diagnosed and laboratory-confirmed. A laboratory-confirmed case of COVID-19 was defined as a positive result on high-throughput sequencing or real-time reverse-transcriptase

polymerase-chain-reaction (RT-PCR) assay of nasal and pharyngeal swab specimens based on the WHO interim guidance (WHO, 2020). The criteria of recovery were normal temperature for at least 3 days, obvious improvement in clinical symptoms, significant absorption of pulmonary inflammation on computer tomography scan and negative tests for SARS-CoV-2 two times in a row with a test interval for at least one day. Individuals tested positive for HIV, HBV, HAV, HCV or syphilis were excluded. All the clinical data were reviewed by a team of physicians from departments of respiratory, intensive care and infectious diseases. Patients without the baseline assessment test were excluded. 23 convalescent COVID-19 patients and one healthy volunteer were included in the study.

PBMC and serum sample preparation

Blood samples were collected using heparin as anticoagulant 3-4 days after donors were discharged from the hospital and separated into plasma and peripheral blood mononuclear cells (PBMCs) by Ficoll-Hypaque gradient centrifugation. Plasmas and PBMCs in freezing media were stored at -80℃. The plasma was heat-inactivated at 56℃ for 1h before use.

Titer measurements by ELISA

384 well plates were coated overnight at 4°C with PBS containing 1 μg/mL of SARS-CoV-2 Spike receptor-binding domain (RBD)-mFc recombinant protein (SinoBiological, catalog # 40592-V05H) or full-length S-his (SinoBiological, catalog # 40589-V08B1) or S1-mFc (SinoBiological, catalog # 40591-V05H1) or S1-his (Kactus, catalog # COV-VM4S1). The

next day the plate was washed 4 times with washing buffer (PBS and 0.05% Tween) and then incubated 1 hour at 37°C in blocking buffer (PBS with 2% BSA). After two washes the plate was incubated for 1 hour at 37 °C with the serum or the positive control ACE2 protein (SinoBiological, catalog # 10108-H08H). The human serum samples were diluted to 1:100 in PBS + 2% BSA followed by 5-fold serial dilutions. The plates were then washed 4 times and incubated for 1 hour in blocking buffer (PBS with 0.05% Tween and 1% BSA) containing diluted (1:5000) secondary antibody (HRP labelled mouse anti-human IgG Fc antibody, Thermo Fisher, catalog # 05-4220, clone name: HP6017) for 1 hour at room temperature. Following this the plate was washed again 4 times and developed in TMB substrate (Biolegend, catalog # 421101) for 5 min before stopping the reaction with the stop solution (Solarbio, catalog # C1058).

Flow cytometry for B cell immune profiling

PBMCs was thawed at 37°C and then centrifuged at 450x g for 8 min. The supernatant was discarded, and the cells resuspended in 200 µL of DMEM (Gibco, catalog # 11995-065). Following the addition of 1µL of Dnase I (Qiagen, catalog # 79254), cells were incubated for 3 min and spun down again. The pellet was resuspended in 20 µL of FcR Blocking Reagent (Miltenyi Biotec, catalog # 130-059-901), incubated for 10 mins and centrifuged. The cells were suspended in 200 µL PBS. 3 µL (1:70 dilution) of anti-CD19 (FITC labeled, eBioscience, catalog # 11-0199-42, clone name: HIB19), anti-CD27 (APC labeled, eBiosciences, catalog # 17-0279-42, clone name: O323), anti-CD38 (PE labeled, eBioscience, catalog # 12-0388-

42, clone name: HB7) or its isotype PE Mouse isotype control (BioLegend, catalog # 400114, clone name: MOPC-21) and FITC labeled mouse IgG1 isotype control (ebioscience, catalog # 11-4714-41, clone name: P3.6.2.8.1) and APC labeled mouse IgG1 isotype control (BD Biosciences, catalog#550854, clone name: MOPC-21) was then added, and incubated for 30 min at room temperature. Following centrifugation, cells were resuspended in a 100 μL of 4% Paraformaldehyde fix solution (PFA; Beyotime, catalog # P0099-500ml). After 10 min the cells were washed twice and finally resuspended in PBS and analyzed using a Cytoflex (Beckman Coulter) flow cytometer. The median fluorescence intensity (MFI) was calculated with FlowJo (version 10.6.0).

Patient sample information for FACS

	Patient #	Cell Number	Viability (%)	Gender
PBMC	Patient 4	2.54×10^5/mL, 200μL	84	Female
PBMC	Patient 20	7.1×10^5/mL, 200μL	90	Male
PBMC	Healthy donor	7.0×10^5/mL, 200μL	92	Male

Isolation of S protein specific B cells

Avi tag and His tag SARS-CoV-2 S protein was expressed in human embryonic kidney cell 293-F (ThermoFisher, catalog# R79007. The cell line was not authenticated.) which was tested negative for mycoplasma contamination. The S protein was purified using HISTRAP HP column (GE, catalog # 17-5248-01) and biotinylated using Biotin-Protein Ligase (GeneCopoeia, catalog # BI001). The B cells were stained with biotinylated S protein and incubated at 4℃ for 1 hour. After incubation, the cells were washed three times with PBS.

Subsequently, the cells were labelled with Streptavidin microbeads (Miltenyi Biotec, catalog # 130-048-101) at 4℃ for 1 hour. After the incubation, the cell suspension was loaded onto a MACS column which is placed on a magnetic field of a MACS separator. The column was washed three times so the magnetically labelled B cells were retained in the column and unlabeled cells passed through. After removing from the MACS separator, the magnetically labelled B cells were eluted. The isolated B cells were counted by using 0.4% (w/v) Trypan blue stain.

Single-cell BCR sequencing

Enriched S protein specific B cells were individually co-compartmentalized in droplets with single barcoded hydrogel beads and lysis and reverse transcription reagents using a microfluidic device as described15. Droplets of ~1 nL volume were formed at 250 s-1. The droplets were collected in a 1.5mL tube containing HFE-7500 (3MTM, catalog # Novec 7500) and 0.1% surfactant (RanBio, catalog # 008-FluoroSurfactant), UV photo-cleaved for 90 seconds (OmniCure ac475-365) and incubated at 50°C for cell lysis and cDNA synthesis. Reverse transcription (RT) of VH and VL mRNAs from single B cells took place in droplet using barcoded primers carrying the T7-SBS12 sequences followed by barcode and gene-specific primer sequences complementary to heavy chain J genes and light chain constant region sequences.

The emulsion containing the barcoded cDNA was broken by adding one volume of 1H,1H,2H,2H-Perfluoro-1-octanol (Sigma-Aldrich, catalog # 370533-25G) after the droplet

RT reaction finished. The pooled, barcoded cDNAs were purified with Agencourt RNA CleanUp beads (Beckman, catalog # A63987) at a 1:1 ratio (vol/vol) twice and eluted in 60 µL DNase- and RNase-free H_2O. The sequencing library was generated by two-step nested PCR using GoTaq Polymerase (Promega, catalog#M7406). In the first PCR, forward primers were priming on the T7 and with reverse primers priming on the VH, Vλ and Vκ leader and framework 1 sequenced of the V genes. In the second PCR, the forward primer appends the Illumina P7 and Illumina index sequences by priming on the SBS12 sequence and the reverse primer appends the Illumina P5 and SBS3 sequence. The approximately 550 bp final PCR products were extracted by agarose gel electrophoresis (Qiagen, catalog#28606). The constructed NGS libraries were sequenced using Illumina MiSeq PE300 which allows sequencing of the entire VH and VL domain as well as the barcode sequence (GeneScript sequencing service supplier) with data varying from 6-12 million reads per samples. The resulting FASTQ data was analyzed by a bioinformatics pipeline enable trimming, merging, barcode extraction and clustering as described(*1*). Briefly, paired-end reads were first trimmed at the 3' end to remove low quality score bases then merged using the program FLASH requiring at least 10bp overlap. The barcodes were extracted from merged reads followed by clustering requiring the DNA sharing at least 93% identify. The consensus sequence was created from clusters by aligning up to 200 sequencings using ClustalO(version1.2), and each antibody sequence was characterized for immunoglobulin content using VDJFasta(version 2.0). We also applied a minimum number of reads 10 for VH and VL. VH-VL pairing was carried out by identifying the most abundant VH and VL

consensus sequence (by the number of reads that contributed to that in each barcode cluster).

Production of recombinant antibody

The DNA of P4A1, P20A2 and P20A3 variable regions of the heavy and light chains were synthesized and cloned into expression plasmids containing the human IgG1 heavy chain and kappa light chain constant regions. The antibodies were expressed in ExpiCHO cell for 8 days after the co-transfection of both heavy and light chain expression plasmids. P4A1-2A was produced by cloning of P4A1 variable regions into expression plasmid containing human IgG4 heavy chain with Fc modifications and expressed in CHO.K1 cells. Antibodies were purified from cell culture supernatants using Protein-A affinity chromatography.

Antibody binding and competition with receptor ACE2

The binding affinity of antibodies to S protein was analyzed by ELISA. 384 well plate (Corning, catalog # 3700), was coated overnight at 4°C with PBS containing 30 µL 20nM of the SARS-CoV-2 Spike S1+S2 ECD, his Tag protein (SinoBiological, catalog # 40589-V08B1). The next day the plate was washed 5 times with washing buffer (PBS and 0.05% Tween) and then incubated 1 hour at room temperature in blocking buffer (PBS with 2% BSA). After 5 washes the plate was incubated with a serial dilution of purified antibodies for 1 hour at room temperature. The plates were then washed 5 times and incubated for 1 hour in blocking buffer (PBS with 0.05% Tween and 1% BSA) containing Mouse anti-Human IgG

Fc HRP labelled (Thermo Fisher, catalog # 05-4220, clone name: HP6017, dilution 1:5000) for 1 hour at room temperature. The plate was then washed again 5 times and incubated with TMB substrate (Biolegend, catalog # 421101) for 5 min before adding the stop solution (Solarbio, catalog # C1058). The OD values at 450nm wavelength were determined using Thermo MultiSkan or MD SpectraMax i3X, data were analyzed with GraphPad Prism (version 8.0.1).

The blocking S1 binding with Vero-E6 cell surface ACE2 receptor was performed using flow cytometry analysis. Vero-E6 cell line (ATCC, CRL-1587) was validated by CoBIOER (http://www.cobioer.com/) and tested negative for mycoplasma contamination. 10 nM SARS-CoV-2 spike S1, mFc tag protein (SinoBiological, catalog # 40591-V05H1) was incubated with a serial dilution of purified antibodies in duplicates at room temperature for 1 hour and then added to Vero E6 cells (105 cells per well). Rabbit anti-mouse IgG Fc-AF647 (Jackson ImmunoResearch, catalog # 315-606-046, 1:800 dilution) was then added before final wash and data acquisition with a Cytoflex flow cytometer (Beckman) and data analysis using FlowJo software (version 10.6.0). Non-linear regression was used to calculate the IC_{50} of the evaluated antibodies with GraphPad Prism (version 8.0.1).

Antibody neutralization activity against pseudovirus

Huh-7 cell line, which expresses ACE2 receptor, was infected with pseudo-virus expressing the full length of SARS-CoV-2 Spike protein and luciferase reporter gene in the presence and absence of serial dilutions of testing antibodies. Viral entry to the cells was quantified

166 using BriteliteTM plus Reporter Gene Assay System. In separate studies, pseudoviruses
167 encoding wild type or different mutant S protein (GenScript, SARS-CoV-2/Wild-type (WT),
168 SARS-CoV-2/D614G, SARS-CoV-2/V367F, SARS-CoV-2/W436R and SARS-CoV-2/D364Y)
169 were incubated with a serial dilution of purified antibodies (starting from 100μg/ml, 3 folds
170 dilution for 8 points) at room temperature for 1 hour. The mixture was then added to ACE2
171 overexpressing HEK293 cells (2×10^4 per well) cultured in DMEM containing 10% FBS in
172 triplicate. Following infection at 37℃ 5% CO_2 for 48 hours, luciferase activity was determined
173 using the Promega Bio-Glo luciferase assay (Promega, catalog # G7491) system. The dose-
174 response curves were plotted with the relative luminescence unit against the sample
175 concentration. Non-linear regression was used to calculate IC_{50} using GraphPad Prism 6.
176
177 **Live virus assay**
178 Microneutralization assays towards live virus were performed as previously described(*2*)
179 with slight modifications. The Vero E6 cell line (ATCC; CRL-1586, Lot#: 60526234; this clone
180 was not authenticated) was tested negative for mycoplasma contamination using a
181 commercial EZ-PCRTM Mycoplasma Test kit (Biological Industries, Beit-Haemek, Israel; 20-
182 700-20; Lot#: 1251719) (data not shown). Briefly, SARS-CoV-2 (strain
183 BetaCoV/Wuhan/WIV04/2019 preserved in National Virus Resource Center under the
184 accession number: IVCAS 6.7512) was mixed with the equivalent volume of culture medium
185 containing serially diluted antibodies and incubated at 37℃ for 1 hour. Then, Vero E6 cells
186 seeded in 96-well plates were incubated with a pre-incubated mixture containing virus at

100 50% tissue-culture infectious doses ($TCID_{50}$) per well and diluted antibodies and were further sustained at 37℃ for 48 hours. Subsequently, cells were fixed with 4% paraformaldehyde diluted in PBS for 15 minutes and penetrated by 0.25% Triton-X 100. After three washes with PBS, cells were blocked at 37℃ for 1 hour using PBS containing 5% BSA, then incubated with in-house prepared anti-SARS-CoV-2 nucleocapsid protein (NP) rabbit serum produced internally at 1:1000 dilution as primary antibody and Goat Anti-Rabbit IgG H&L (Alexa Fluor® 488) (1:500 dilution, Abcam, Cambridge, UK; ab150077; Lot#: GR3244688-2) as the secondary antibody. Cell nuclei were stained using Hoechst 33258 (Beyotime, Shanghai, China; C1018). Images were taken, and numbers of nuclei and cells infected with viruses were counted, respectively, using an Operetta CLSTM system (PerkinElmer, Waltham, USA). Inhibition was calculated by (total nuclei-infected cells)/ total nuclei x 100%. Fifty percent neutralization dose (ND_{50}) were calculated with GraphPad Prism 8.0.

Surface plasmon resonance analysis of wild-type or mutant RBD/S1 binding.

SPR experiments were performed using Biacore T200 system (GE Healthcare). In brief, experiments were performed at 25°C in HBS-EP+ buffer. The antibody was immobilized onto a protein A sensor chip (GE healthcare, catalog#29139131-AA). Serially diluted SARS-CoV-2 RBD (WT, AcroBiosystems, catalog#SPD-C52H3), RBD (N354D/D364Y, AcroBiosystems, catalog#SPD-S52H3), RBD (R408I, AcroBiosystems, catalog#SPD-S52H8), RBD (W436R, AcroBiosystems, catalog#SPD-S52H7), RBD (V367F, AcroBiosystems, catalog#SPD-

S52H4) or SARS-CoV-2 spike S1 domain (D614G, Sino Biological, catalog#40591-V08H3) were injected through flow cells for 60s of association followed by a 150s dissociation phase at a flow rate of 30 μL min−1. Prior to the next cycle, the sensor surface was regenerated with Glycine-HCl (pH 1.5) for 30s at a flow rate of 30 μL min−1. KD values were calculated using the 1:1 binding kinetics model.

Protein expression and purification

The codon-optimized wild type cDNA of SARS-CoV-2 RBD (residues 333–530) was synthesized. The SARS-CoV-2 RBD with a C-terminal 8×His tag for purification was cloned into pAcgp67 vector with BamH Ⅰ and Not Ⅰ restriction sites using the cloning primers. The sequences of the primers were: 5'-TCTCCTACATCTACGCCGACGGATCCACCAACCTCTGCCCTTTCGGT-3' (forward), 5'-TGGTGATGGTGGTGATGATGTGCGGCCGCACTCTTCTTTGGCCCGCATA -3' (reverse). The accuracy of the inserts was verified by sequencing.

The SARS-CoV-2 RBD was expressed using the Bac-to-Bac baculovirus system. The construct was transformed into bacterial DH5α component cells, and the extracted bacmid was then transfected into Sf9 cells using Cellfectin II Reagent (Invitrogen). The low-titer viruses were harvested and then amplified to generate high-titer virus stock. The viruses and Endo H, Kifunensine were co-infected Hi5 cells at a density of 2×10^6 cells/ml. The supernatant of cell culture containing the secreted removal of glycosylated RBD was harvested 72 h after infection, concentrated and RBD was captured by Ni-NTA resin (GE

Healthcare). The resin was washed 5-6 times with 30 mL of wash buffer (25 mM Tris, 150 mM NaCl, 40 mM imidazole, pH 7.5), the target protein was eluted with elution buffer containing 25 mM Tris, 150 mM NaCl, 500 mM imidazole, pH 7.5. The protein was further purified on a Superdex S75 (GE Healthcare) column equilibrated with 25 mM Tris, 150 mM NaCl, pH 7.5. SDS-PAGE analysis revealed over 95% purity of the final purified recombinant protein. Fractions from the single major peak were pooled and concentrated to 15 mg/mL RBD were collected.

Crystallization

The SARS-CoV-2 RBD protein and P4A1-Fab fragment were mixed at a molar ratio of 1.5:1. The mixture was incubated on ice for 1 h and further purified by Superdex S75 (GE Healthcare). 7 mg/mL and 10 mg/mL of SARS-CoV-2 RBD/Fab proteins were used for crystal screening by vapour-diffusion sitting-drop method at 16 °C, including the Index, Crystal Screen, PEG/Ion, SaltRX from Hampton Research and wizard Ⅰ-Ⅳ from Emerald BioSystems.

The rode-like crystals appeared after two days at the mother liquid containing 20% w/v PEG 3350, 0.2 M potassium citrate tribasic. Further optimization with additive and hanging-drop vapour-diffusion method was performed, the final optimized diffraction crystals at the mother liquid containing 20% w/v PEG 3350, 0.2 M potassium citrate tribasic by the hanging-drop vapour-diffusion method. Crystals were dehydrated and cryo-protected in 4M Sodium formate solution and cooled in a dry nitrogen stream at 100 K for X-ray data collection.

X-ray data collection, processing, and structure determination

Diffraction data were collected at the Shanghai Synchrotron Radiation Facility (SSRF) BL17U1 (wavelength, 0.97915 Å) at 100K. All data sets were processed using the HKL3000 package(*3*). Structures were solved by molecular replacement using PHASER(*4*) with the SARS-CoV-2 RBD structure (PDB ID: 6M0J) (*5*) and the structures of the Fab fragment available in the PDB with the highest sequence identities. The initial model was built into the modified experimental electron density using COOT (*6*) and further refined in PHENIX(*7*). Model geometry was verified using the program MolProbity. Structural figures were drawn using the program PyMOL(*8*) (http://www.pymol.org). Epitope and paratope residues, as well as their interactions, were identified by accessing PISA (http://www.ebi.ac.uk/pdbe/prot_int/pistart.html) at the European Bioinformatics Institute.

Binding affinity to FcγRs and C1q

The binding affinity of P4A1-2A as well as its IgG1 form for different human FcγRs, FcRn was tested by SPR using Biacore 8K (GE Healthcare). FcγRI, FcγRIIa (H131), FcγRIIb, FcγRIIIa (V158) (all from AcrobioSystems) were captured on the activated CM5 sensor chips, followed by flow-through of 10 concentrations of serial diluted P4A1 (IgG1) or P4A1-2A (IgG4) antibodies. For FcRn binding, P4A1 or P4A1-2A were captured on the activated CM5 sensor chips followed by flow-through of 10 concentrations of serial diluted FcRn (AcrobioSystems). The sensor chips were regenerated by flow-through of 10 mM glycine

(pH 1.5).

Antibody binding to C1q was tested by ELISA, with P4A1 or P4A1-2A antibodies to coat the plate overnight at 4°C, followed by incubation with 11 concentration of half-log titrated human C1q (Complement Technology), then incubation with secondary antibody Sheep anti-human C1q Ab-HRP (Complement Technology), before TMB substrate was added and absorbance at 450 nm was determined using a SpectraMax Plus384 microplate reader.

RT-PCR

Total RNA was extracted from organs with an RNeasy Mini Kit (Qiagen, USA) and PrimerScript RT Reagent Kit (TaKaRa, Japan). The forward and reverse primers targeting the SARS-CoV-2 NP gene for RT-PCR were 5'-GGGGAACTTCTCCTGCTAGAAT-3' and 5'-CAGACATTTTGCTCTCAAGCTG-3', respectively. RT-PCR was performed under the following reaction conditions: 42℃ for 5 min, 95℃ for 10 s, and 40 cycles of 95℃ for 10 s and 60℃ for 30 s.

Pharmacokinetic (PK) analysis

Six (6, 3/sex) naïve cynomolgus monkeys were enrolled in the study and administered with P4A1-2A at 10 mg/kg by single intravenous infusion. Blood samples PK analysis were collected at pre-dose, and different time-points after the treatment. Serum concentrations of P4A1-2A were determined by ELISA.

Safety evaluation

Cynomolgus monkeys (3-5 years old, 2.2 to 3.6 kg for females and 2.3 to 5.2 kg for males, sourced from GuangDong Blooming-Spring Biological Technology Development Co., Ltd.) were randomly assigned to 3 groups of 5/sex/group and given P4A1-2A at 0, 50, or 300 mg/kg/dose on Day 1 and Day 8 by intravenous (IV) infusion. Animals were monitored daily with blood samples collected at different time-point for various testing. Animals were euthanized on Day 15 to examine thoroughly for any potential toxicity.

In vivo efficacy in SARS-CoV-2 infection model in rhesus monkey

Nine rhesus monkeys (RMs, three males, six females; 6–7 years of age, 5.3-7.3 kg, sourced from Hubei Tianqin Biotech Company), were inoculated with SARS-CoV-2 virus (BetaCoV/Wuhan/WIV04/2019)(*2*) at 1×10^5 $TCID_{50}$ intratracheally under anesthesia on Day 0. Animals were randomized into 3 groups (1 male and 2 females in each group) and receive a single intravenous (i.v.) treatment of Isotype control W332-1.80.12.xAb.hIgG4 (sourced from Wuxi Biologics, Co. Ltd.) at 50 mg/kg, or P4A1-2A at 10 or 50 mg/kg, respectively, one day after viral infection. The RMs were observed twice daily with detailed recording of clinical signs. Swab samples of the oropharyngeal, nasal turbinate, and rectal regions, as well as whole blood (in K2EDTA tubes), were collected at 0-7 days post-infection (d.p.i.). To confirm the pathogenesis and injury in the respiratory system, one animal from each treatment groups were sacrificed at 5-7 d.p.i., respectively. The trachea, right bronchus, left bronchus, all six lung lobes and other tissue organs were collected on the day of

euthanization for various pathological, virological analyses. Viral loads in swabs and tissues were determined and pathological examination was conducted as previously described (*9*).

Data availability

Protein coordinate and structure factors are deposited in the RCSB Protein Data Bank under ID 7CJF. All data is available in the main text or the supplementary materials.

Extended Figures and Tables

Figure S1

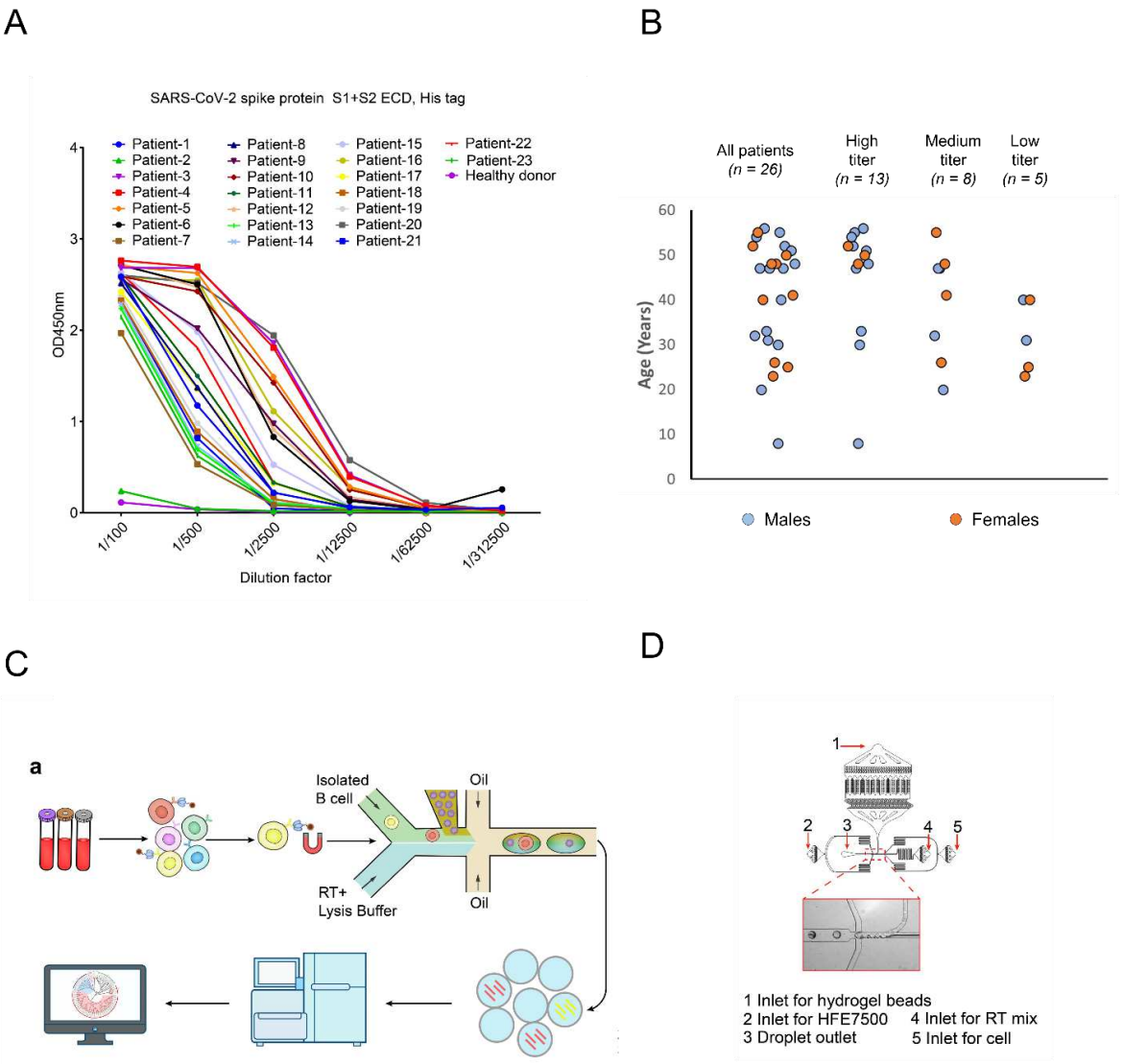

Fig.S1. Analyses of plasma responses to SARS-CoV-2 proteins and antibody identification from convalescent patients using single cell sequencing.

(A) Serums from 23 convalescent patients and one healthy donor were analyzed for their binding abilities to the SARS-CoV-2 spike protein using ELISA. (B) Classification of patient samples into high (>2500), medium (500-2500), and low (<500) titer categories. (C)

328 Schematic diagram of the antibody identification from convalescent patients using single cell
329 sequencing. SARS-CoV-2 S protein binding B cells were isolated from PBMC of
330 convalescent patients with magnetic beads that conjugated with biotinylated S protein as
331 probes. The isolated cells were individually co-compartmentalized in droplets along with
332 lysis buffer, reverse transcriptase and one hydrogel bead. Each hydrogel bead carried VH
333 and VL specific oligos tagged with a unique barcode. The resulting cDNAs from one cell
334 carried an identical barcode. The barcoded cDNAs were sequenced to identify cognate
335 heavy and light chain pairs. (D) The design of the microfluidics chip for co-
336 compartmentalization of single cells and single hydrogel bead in droplets.
337

Figure S2

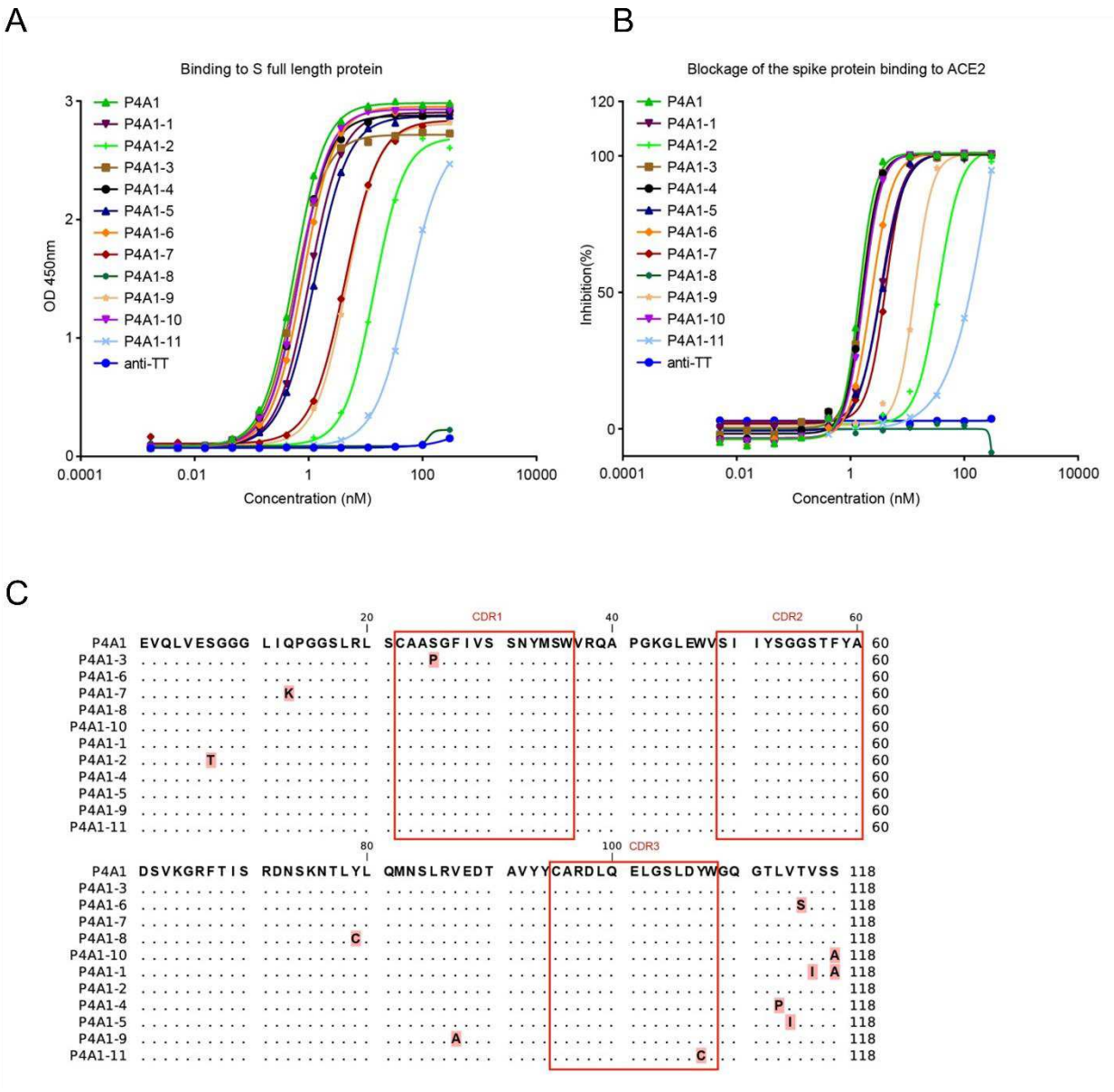

Fig.S2. Identification and characterization of somatic variants of antibody P4A1.

Eleven heavy chain sequences closely related to P4A1 were bioinformatically identified from NGS results. These P4A1-class heavy chains were reconstituted with the light chain from P4A1 and numbered P4A1-1 to P4A1-11. (A) Binding of the antibodies to the full-length S protein was evaluated by ELISA. (B) Blocking the binding of S1 protein to Vero E6 cell line

by antibodies was evaluated by flow cytometry. (C) The amino acid sequences of the P4A1-class antibodies were aligned.

Figure S3

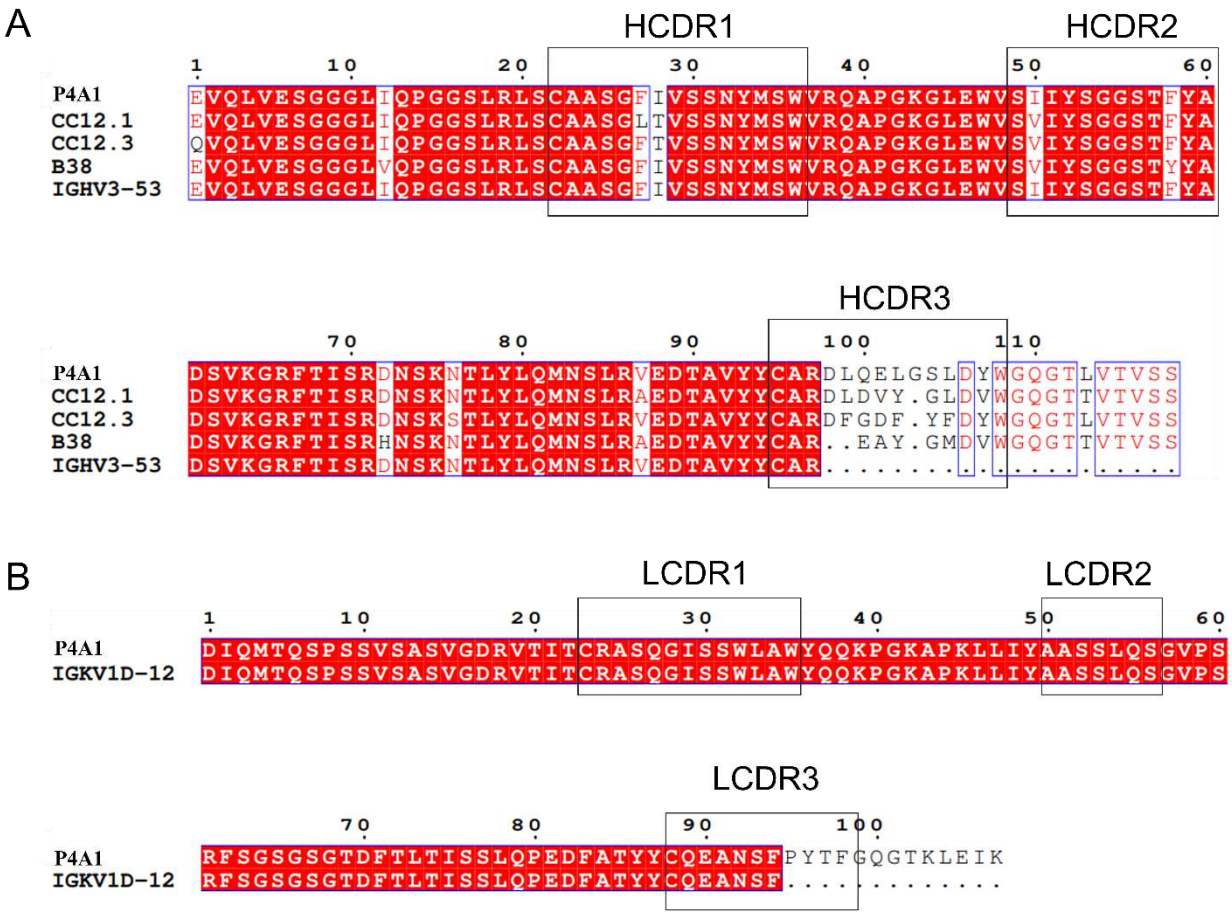

C

Antibody	Heavy chain	Light chain
P4A1	IGHV3-53	IGKV1-12
CC12.1	IGHV3-53	IGKV1-9
CC12.3	IGHV3-53	IGKV3-20
B38	IGHV3-53	IGKV1-9

Fig.S3. Sequence alignment of P4A1 to other reported antibodies from the IGHV3-53 germline. (A) Alignment of the heavy chain variable domain sequence of P4A1 with CC12.1, CC12.3, B38 and the germline IGHV3-53 sequence. (B) Alignment of the light chain variable domain sequence of P4A1 with the germline IGKV1D-12 sequence. (C) Germline usage comparison of the heavy chain and light chain discussed in this paper.

Figure S4

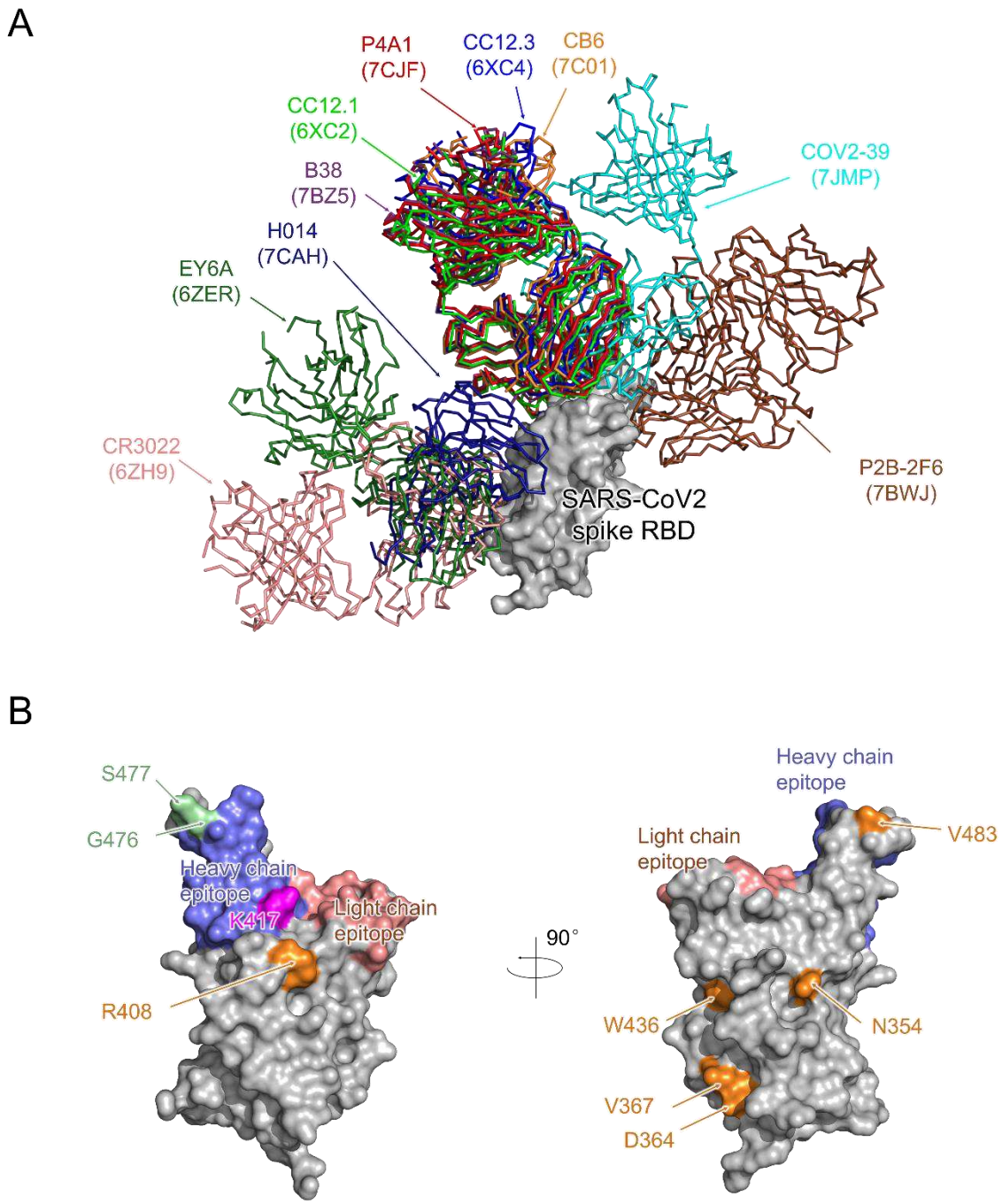

Fig.S4. Structural comparison of the binding mode among several reported RBD-specific neutralizing antibodies from various germlines. (A) Superimpose of P4A1 (red, PDB 7CJF), CC12.1 (green, PDB 6XC2), CC12.3 (blue, PDB 6XC4), B38 (purple, PDB 7BZ5), CB6 (orange, PDB 7C01), COV2-39 (cyan, PDB 7JMP), H014 (deep blue, PDB

7CAH), EY6A (forest green, PDB 6ZER), CR3022 (salmon red, PDB 6ZH9), P2B-2F6 (brown, PDB 7BWJ), to SARS-CoV-2 spike glycoprotein RBD (gray). (B) Surface representation of several clinical isolates with Spike RBD mutations. The SARS-CoV-2 RBD is colored in gray and displayed in surface representation. The epitope of P4A1 heavy chain (slate blue), light chain (salmon red), residue K417 (pink) are displayed and colored as Figure2. The clinic mutations G476 and S477, which located at the edge of the P4A1 epitope are colored in pale green. The clinic mutations N354, D364, V367, R408, W436, and V483, which are adjacent to the epitope residues or on the opposite side of the P4A1 epitope, are colored in orange.

Figure S5

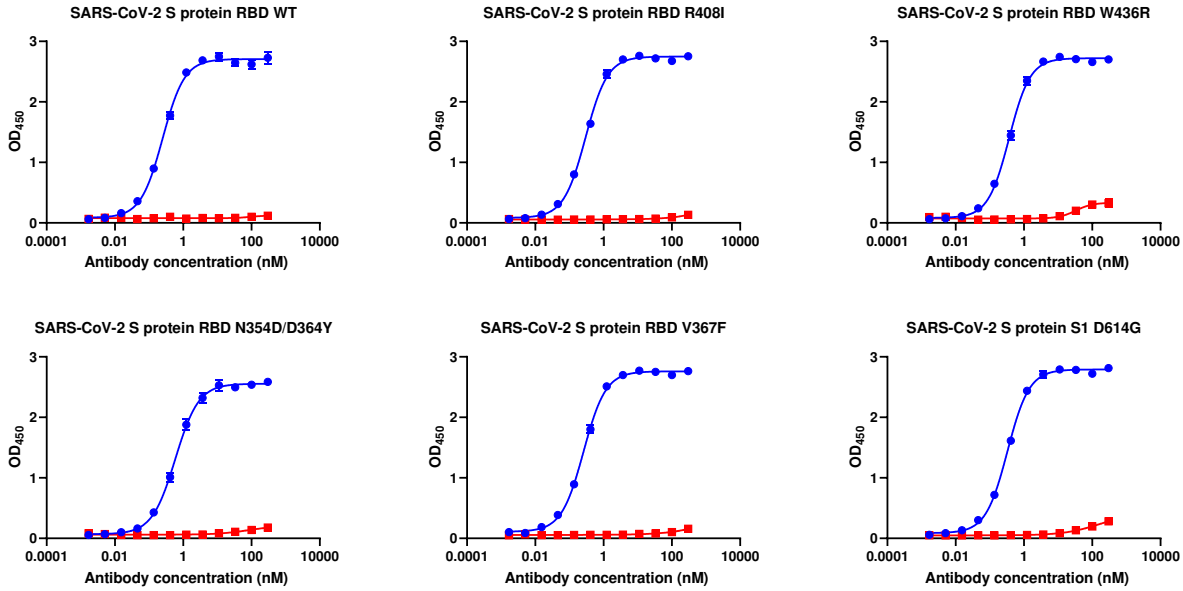

	WT	R408I	W436R	N354D/D364Y	V367F	D614G
EC_{50} (nM)	0.250	0.299	0.369	0.587	0.259	0.329

Fig. S5. The binding of the P4A1-2A (blue) or isotype control (red) antibodies to the SARS-CoV-2 S protein RBD or S1 variants was determined by ELISA. The 384-well plates were coated with 20 nM of the respective SARS-CoV-2 S protein RBD/S1 variants. The binding of P4A1-2A or isotype control antibodies (12 concentrations obtained by 3-fold serial dilutions of a 300 nM antibody stock solution, in triplicate) was detected by goat F(ab')2 anti-human IgG (H+L)-HRP. Table: summary of EC_{50}s calculated by non-linear regression of the data.

384 **Figure S6**

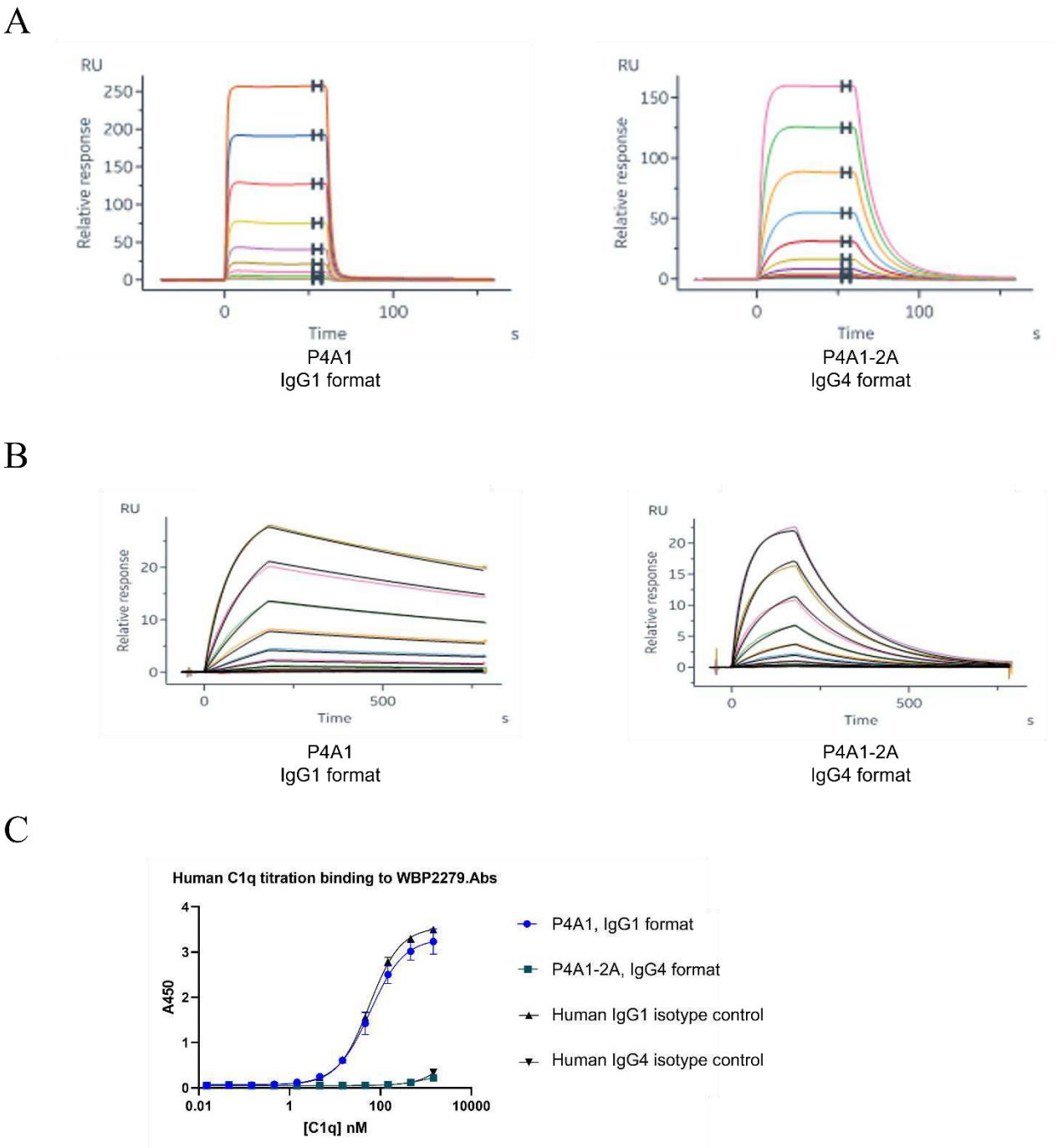

385

386 **Fig.S6. Binding of P4A1 (IgG1 form) and P4A1-2A (IgG4 form) to FcRn (A), FcγRI (B)**

387 **by SPR using Biacore 8K and C1q (C) by ELISA.** Assays are detailed in material and

388 methods.

389

Figure S7

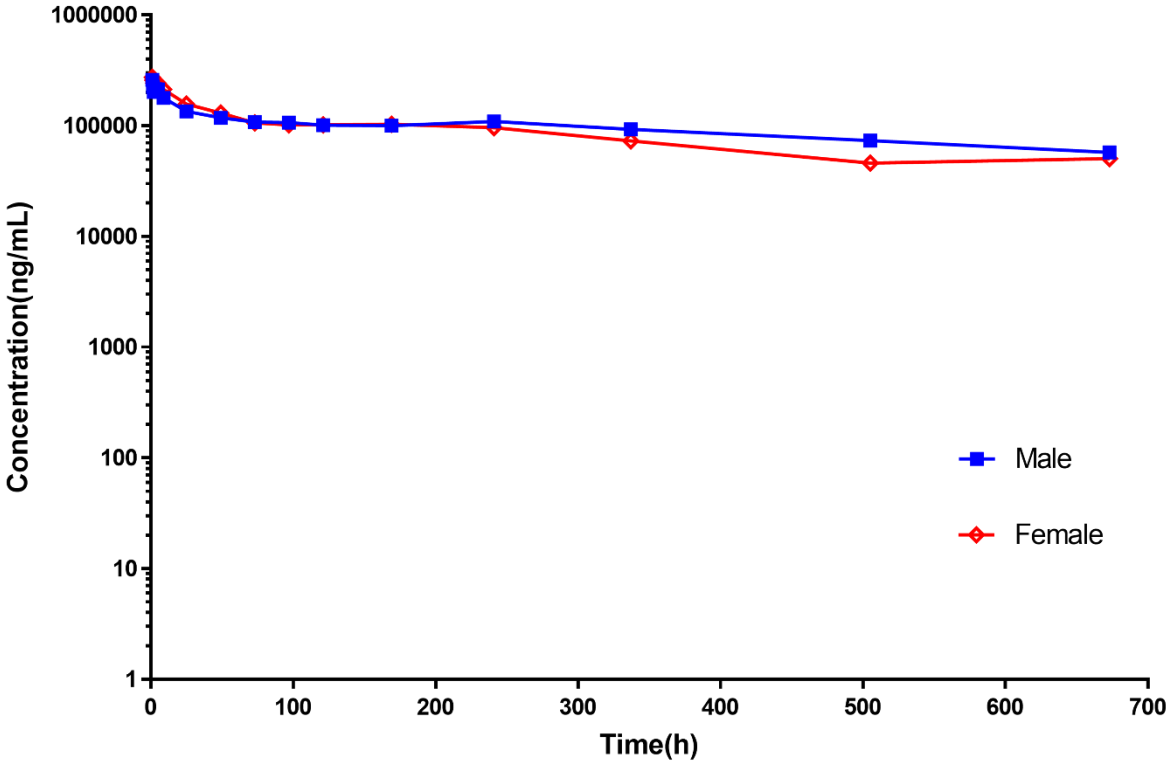

PK Parameter	Mean (Male)	Mean (Female)
C_{max} (ng/mL)	259000	273000
C_{last} (ng/mL)	27700	13000
T_{max} (h)	1.0833	1.0833
$T_{1/2}$ (h)	586	332
$AUC_{0\text{-last}}$ (ng.h/mL)	88200000	66700000

Fig.S7. Mean serum P4A1-2A concentration in cynomolgus monkeys. Male and female cynomolgus monkeys (N=3/sex) were treated with a single i.v. infusion administration at 10 mg/kg P4A1-2A in 60 mins infusion time. Blood samples collected at different timepoints and serum concentrations of P4A1-2A were determined with ELISA. PK parameters derived are listed in the lower panel.

Figure S8

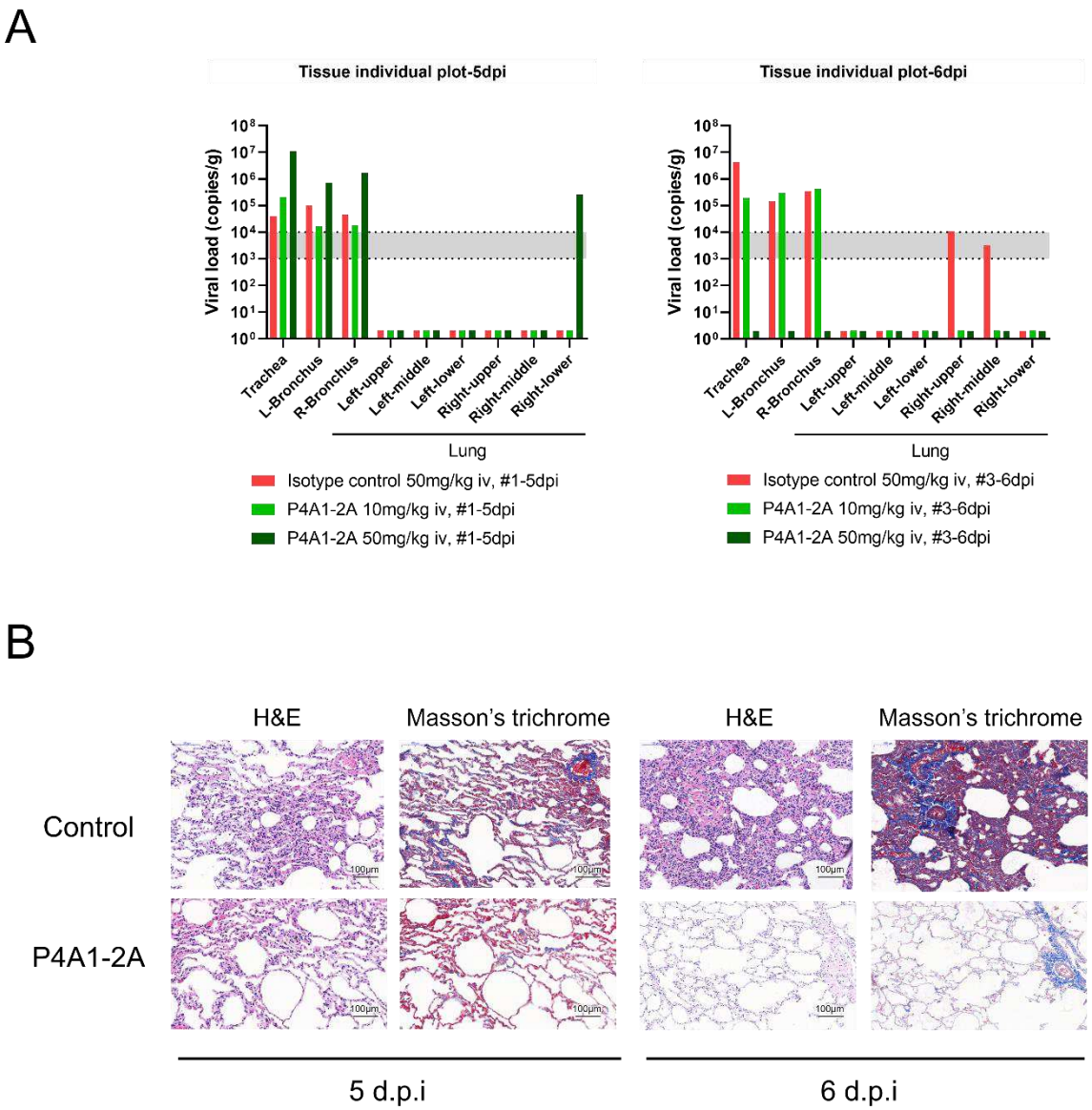

Fig.S8. Viral load and histopathology in lung tissue in the rhesus macaque model of SARS-CoV-2 infection 5 and 6 d.p.i. (A) Viral load in the respiratory tissues (including trachea, left and right bronchus, and all six lung lobes) collected at necropsy on 5 (left) or 6 (right) days post-infection (d.p.i) were tested by RT-qPCR. (B) Representative images of histopathology in lung tissue from isotype control or P4A1-2A 50 mg/kg treated animals (collected at 5 and 6 d.p.i).

411 **Table S1. Data collection and refinement statistics.**

Wavelength	0.97915
Resolution range	36.16 - 2.108 (2.183 - 2.108)
Space group	C 2 2 21
Unit cell	85.958 148.575 144.655 90 90 90
Total reflections	475973
Unique reflections	48014 (4316)
Multiplicity	9.6 (9.7)
Completeness (%)	89.21 (81.11)
Mean I/sigma(I)	23.5 (2.3)
Wilson B-factor	32.62
R-merge	0.091 (0.800)
R-meas	0.097 (0.844)
R-pim	0.031 (0.264)
CC1/2	0.996 (0.895)
Reflections used in refinement	47909 (4316)
Reflections used for R-free	1991 (185)
R-work	0.1858 (0.2309)
R-free	0.2284 (0.2616)
Number of non-hydrogen atoms	5466
macromolecules	4861
ligands	14
solvent	591
Protein residues	793
RMS(bonds)	0.007
RMS(angles)	0.95
Ramachandran favored (%)	97.1
Ramachandran allowed (%)	2.9
Ramachandran outliers (%)	0
Rotamer outliers (%)	0.55
Clashscore	4.8
Average B-factor	39.13
macromolecules	37.67
ligands	82.89
solvent	50.16
Number of TLS groups	1

412 Statistics for the highest-resolution shell are shown in parentheses.

413

414 **Table S2. Residues contributed to interaction between P4A1/SARS-CoV-2-RBD.**

SARS-CoV-2 RBD	Distance (Å)			P4A1 Antibody
Hydrogen Bonds				
SER 477 [N]	3.1			VH:GLY 26 [O]
LYS 458 [NZ]	2.7			VH:SER 30 [O]
TYR 473 [OH]	2.8			VH:SER 31 [O]
TYR 449[OH]	4.0			VH: SER 31[OG]
LYS 458 [NZ]	3.1			VH:SER 53 [O]
TYR 421 [OH]	3.4			VH:SER 53 [OG]
LYS 417 [NZ]	2.7			VH: GLN 100 [OE1]
TYR 453 [OH]	2.4			VH: GLU 101 [OE1]
ASP 420 [OD2]	2.5			VH:SER 56 [OG]
TYR 421 [OH]	3.6			VH:SER 53 [N]
TYR 421 [OH]	2.9			VH:GLY 54 [N]
LEU 455 [O]	2.8			VH:TYR 33 [OH]
ARG 457 [O]	2.6			VH:SER 53 [OG]
ALA 475 [O]	3.2			VH:ILE 28 [N]
ALA 475 [O]	2.9			VH:ASN 32 [ND2]
ASN 487 [OD1]	2.9			VH:ARG 97 [NH1]
TYR 489 [OH]	3.4			VH:ARG 97 [NH2]
GLY 502 [N]	3.0			VL:GLY 28 [O]
ARG 403 [NH1]	2.9			VL:ASN 92 [O]
ARG 403 [NH2]	3.1			VL:ASN 92 [O]
TYR 505 [OH]	2.7			VL:SER 93 [OG]
ASN 501 [OD1]	3.2			VL:SER 30 [N]
GLY 496 [O]	3.0			VL:SER 30 [OG]
ASN 501 [OD1]	3.0			VL:SER 30 [OG]
GLN 498 [OE1]	3.4			VL:SER 67 [OG]
TYR 505 [OH]	3.6			VL:SER 93 [N]
Salt Bridge				
LYS 417 [NZ]	3.1			VH: GLU 101 [OE2]
Solvent Hydrogen Bond Bridge				
GLY 476 [O]	3.0	W740	3.0	VH: SER 31 [OG]
TYR 505 [OH]	2.8	W388	2.8	VL: TRP 32[O]
TYR 505 [OH]	2.8	W388	3.1	VL: ALA 91 [N]
TYR 505 [OH]	2.8	W388	2.9	VL: ASN 92 [N]

415

416

Reference.

1. A. Gérard *et al.*, High-throughput single-cell activity-based screening and sequencing of antibodies using droplet microfluidics. *Nature Biotechnology* **38**, 715-721 (2020).
2. P. Zhou *et al.*, A pneumonia outbreak associated with a new coronavirus of probable bat origin. *Nature* **579**, 270-273 (2020).
3. W. Minor, M. Cymborowski, Z. Otwinowski, M. Chruszcz, HKL-3000: the integration of data reduction and structure solution--from diffraction images to an initial model in minutes. *Acta Crystallogr D Biol Crystallogr* **62**, 859-866 (2006).
4. A. J. McCoy *et al.*, Phaser crystallographic software. *J Appl Crystallogr* **40**, 658-674 (2007).
5. J. Lan *et al.*, Structure of the SARS-CoV-2 spike receptor-binding domain bound to the ACE2 receptor. *Nature* **581**, 215-220 (2020).
6. P. Emsley, B. Lohkamp, W. G. Scott, K. Cowtan, Features and development of Coot. *Acta Crystallogr D Biol Crystallogr* **66**, 486-501 (2010).
7. P. D. Adams *et al.*, PHENIX: a comprehensive Python-based system for macromolecular structure solution. *Acta Crystallogr D Biol Crystallogr* **66**, 213-221 (2010).
8. Schrodinger, LLC. (2015).
9. C. Shan *et al.*, Infection with novel coronavirus (SARS-CoV-2) causes pneumonia in Rhesus macaques. *Cell Res* **30**, 670-677 (2020).

Figures

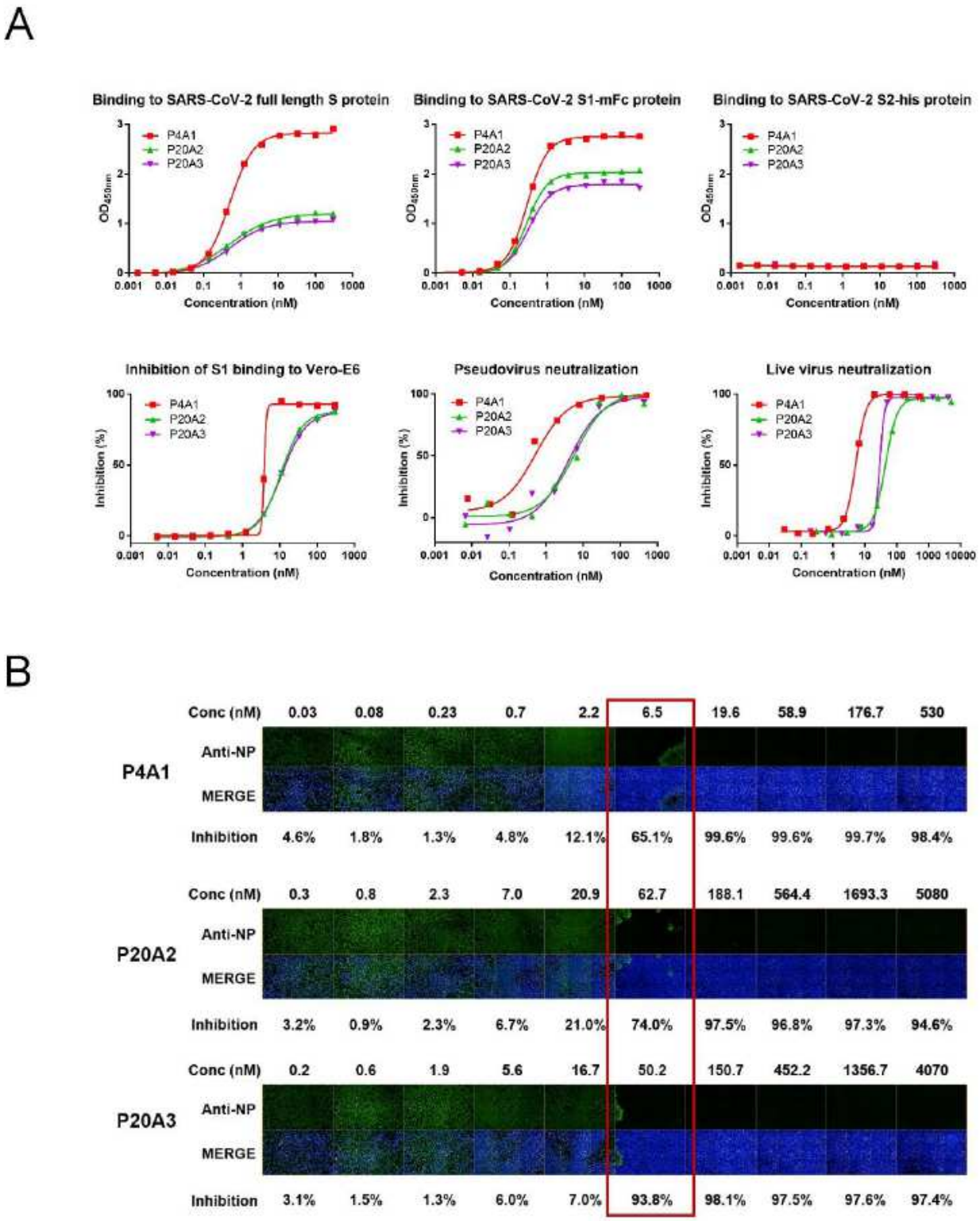

Figure 1

Characterization of neutralizing antibodies from convalescent patients. (A) Characterization of SARS-CoV-2 S protein specific antibodies. (upper panels) Binding of antibodies to the full-length S protein, S1 protein and S2 protein were evaluated by ELISA. (lower left panel) Blockage of the binding of SARS-CoV-2

spike S1 protein to Vero E6 cell line by antibodies evaluated by flow cytometry. (Lower middle panel) Pseudovirus neutralization assay in Huh-7 cell line. (lower right panel and B) SARS-CoV-2 live virus neutralization assay. (B) Images of Vero E6 cells infected SARS-CoV-2 treated with antibodies of different concentrations.

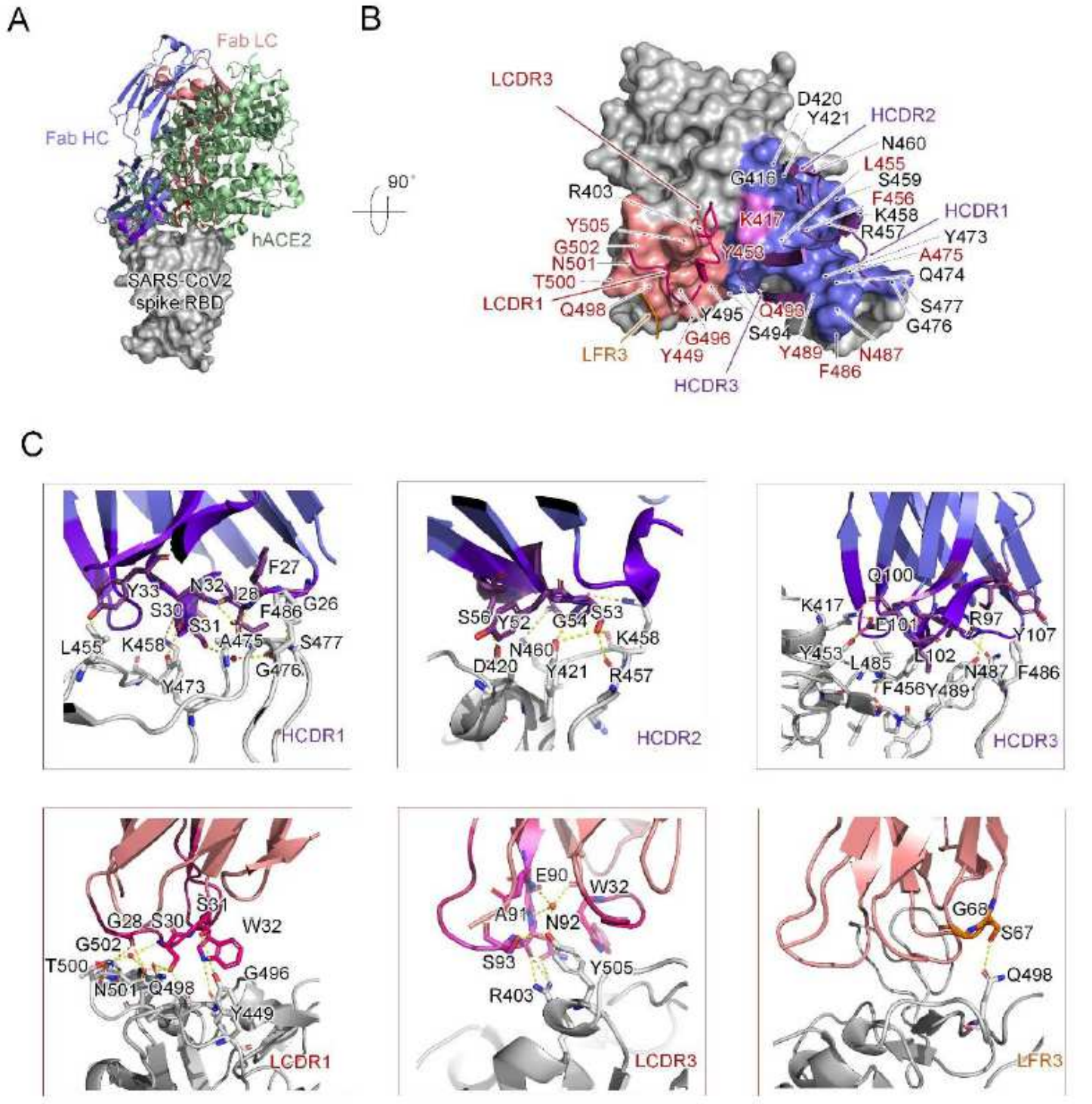

Figure 2

Structural analysis of P4A1 Fab and SARS-CoV-2 RBD complex. (A) The overall P4A1-Fab-RBD complex structure superimposed with the hACE2-RBD complex. The P4A1 heavy chain (colored slate blue), light

chain (colored salmon red) and hACE (colored pale green) are displayed in cartoon representation. The SARS-CoV-2 RBD is colored in gray and displayed in surface representation. (B) The epitope of P4A1 shown in surface representation. The CDR loops of heavy chain (HCDR) and light chain (LCDR) are colored in purple and magenta, respectively. The epitopes from the heavy chain and light chain are colored in slate blue and salmon red, respectively. The only residue K417, which contacts with both heavy chain and light chain is colored in pink. The light chain frame region 3 (LFR3) is colored in orange. The identical residues on RBD shared in P4A1 and hACE2 binding are labelled in red. The residues are numbered according to SARS-CoV-2 RBD. (C) The detailed interactions between SARS-CoV-2 RBD with HCDR, LCDR and LFR3. The residues are shown in sticks with identical colors to (B).

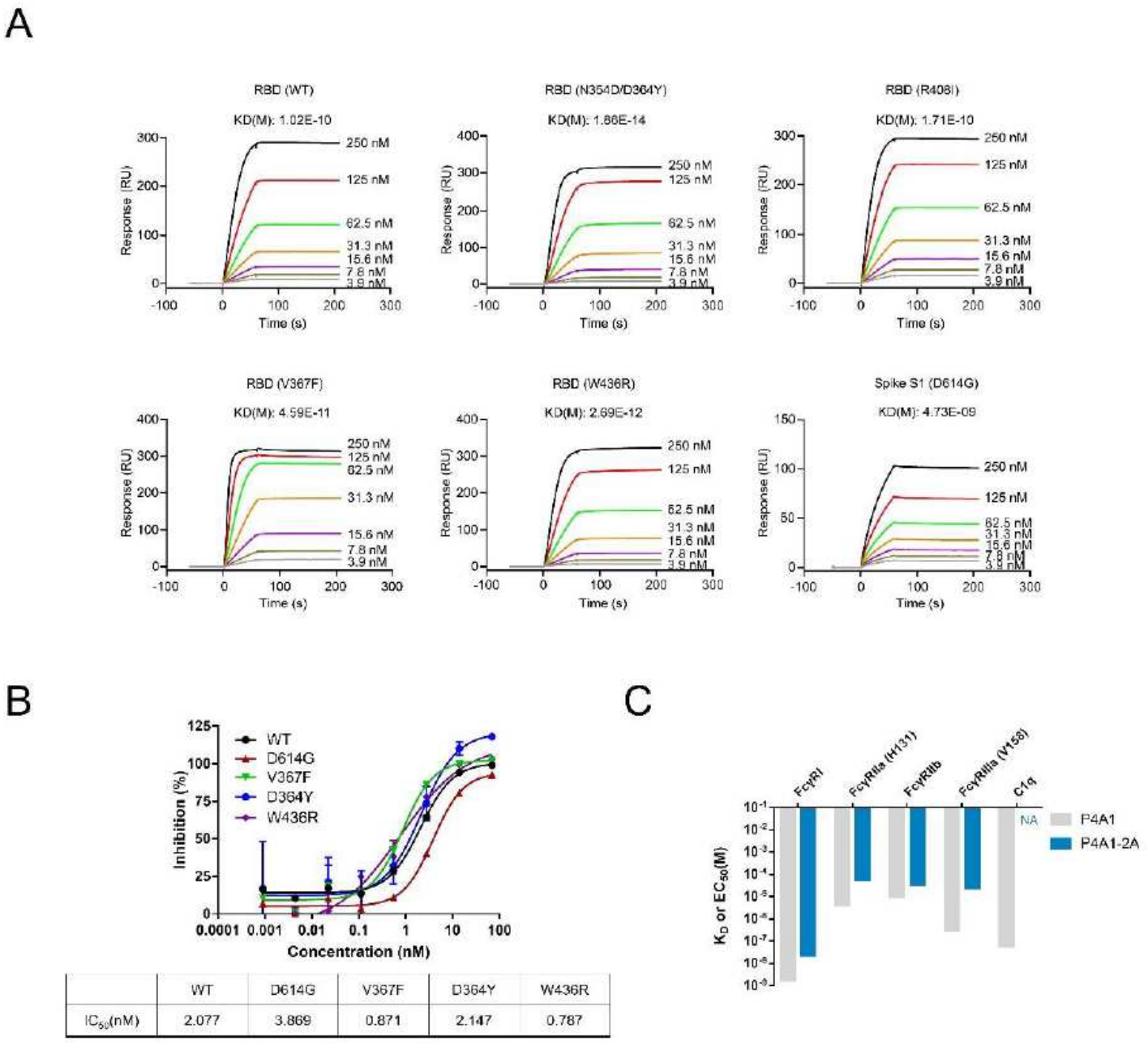

	WT	D614G	V367F	D364Y	W436R
IC_{50}(nM)	2.077	3.869	0.871	2.147	0.787

Figure 3

The activities of IgG4 antibody P4A1-2A to different SARS-CoV-2 S protein mutants, FcγRs and C1q. (A) Binding of antibody P4A1 to SARS-CoV-2 S protein N354D/D364Y, R408I, W436R, V367F or D614G mutants determined by SPR. (B) Pseudo virus neutralization assay in hACE2 overexpressing HEK293 cells. (C) The binding affinity of P4A1 and P4A1-2A for different human FcγRs and complement C1q.

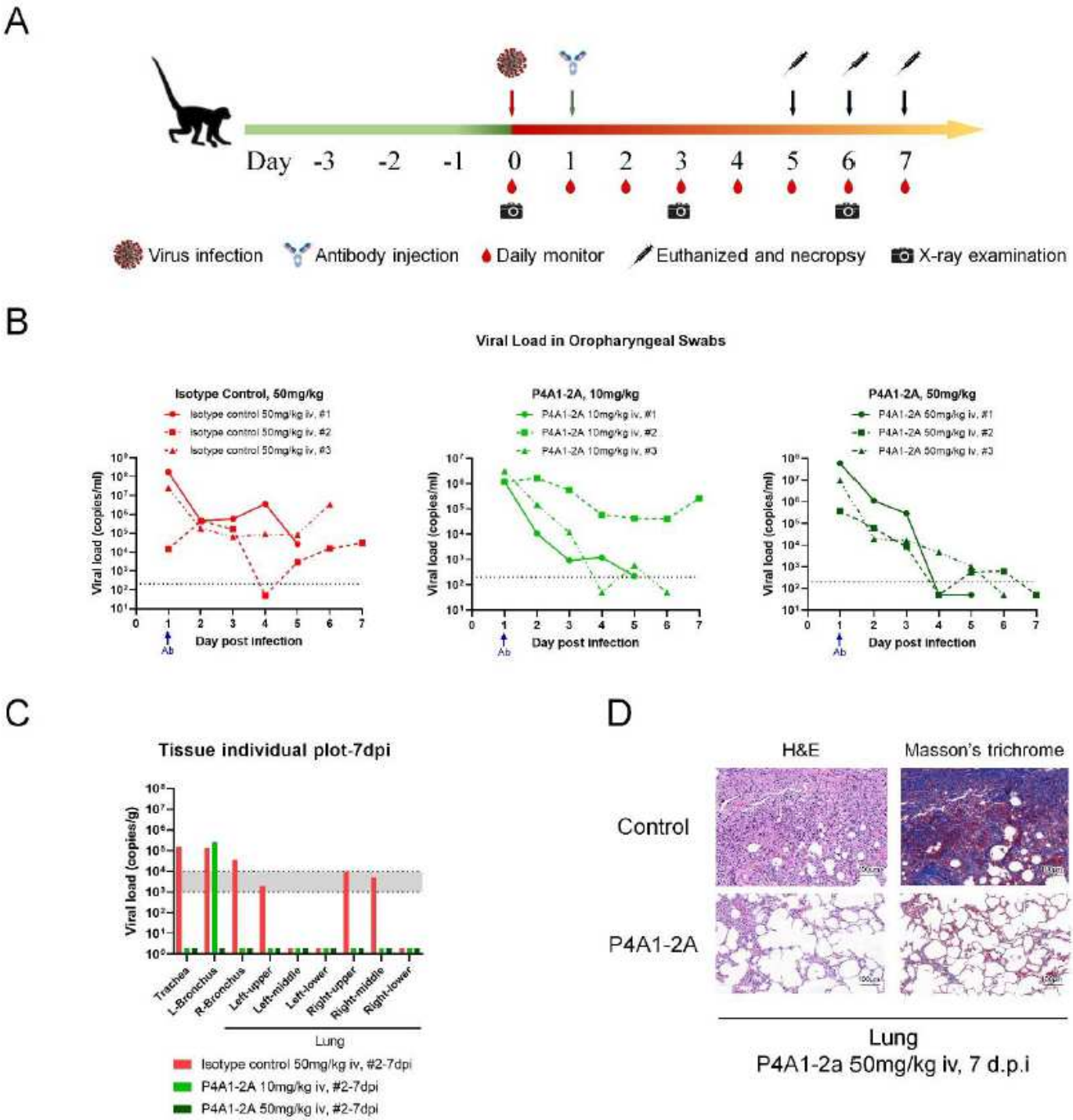

Figure 4

Therapeutic efficacy of in the rhesus macaque model of SARS-CoV-2 infection. (A) Experimental design for therapeutic testing of P4A1-2A in the rhesus macaque. (B) Viral load in oropharyngeal swabs tested

by RT-qPCR were monitored for 7 days. (C) Viral load in the respiratory tissues (including trachea, left and right bronchus, and all six lung lobes) collected at necropsy on 7 days post-infection (d.p.i) were tested by RT-qPCR. (D) Representative images of histopathology in lung tissue from isotype control or P4A1-2A 50 mg/kg treated animals (collected at 7 d.p.i).

Supplementary Files

This is a list of supplementary files associated with this preprint. Click to download.

- NCOMMS2041615T.pdf
- NCOMMS2041615TvalreportfullP1.pdf